2020-06

Development of a fast and accurate method for the segmentation of diabetic foot ulcer images

Mwawado, Rehema H.

NM-AIST

DEVELOPMENT OF A FAST AND ACCURATE METHOD FOR THE SEGMENTATION OF DIABETIC FOOT ULCER IMAGES

Rehema H. Mwawado

A Dissertation Submitted in Partial Fulfilment of the Requirements for the Degree of Master's in Information and Communication Science and Engineering of the Nelson Mandela African Institution of Science and Technology

Arusha, Tanzania

June, 2020

ABSTRACT

Globally, Diabetic Foot Ulcers (DFUs) are among the major sources of morbidity and death among people diagnosed with diabetes. Diabetic foot ulcers are the leading diabetes-related complications that result in non-traumatic lower-limb amputations among these patients. Being a serious health concern, DFUs present a significant therapeutic challenge to specialists, particularly in countries with limited health resources and where the vast majority of patients are admitted to healthcare facilities when the ulcers have fully advanced.

Clinical practices currently employed to assess and treat DFU are mostly based on the vigilance of both the patient and clinician. These practices have been proved to experience major limitations which include less accurate assessment methods, time-consuming diagnostic procedures, and relatively high treatment costs. Digital image processing is thus a potential solution to address issues of the inaccuracy of visual assessment as well as minimizing consecutive patient visits to the clinics.

Image processing techniques for ulcer assessment have thus been a center of study in various works of literature. In the available works of literature, these methods include measuring the ulcer area as well as using a medical digital photography scheme. The most notable drawbacks of such approaches include system complexity, complex-exhaustive training phases, and high computational cost.

Inspired by the weaknesses of the existing techniques, this study proposes a segmentation method that incorporates a hybrid diffusion-steered functional derived from the Total variation and the Perona-Malik diffusivities, which have been reported that they can effectively capture semantic features in images. Empirical results from the experiments that were carried out in the MATLAB environment show that the proposed method generates clearer segmented outputs with higher perceptual and objective qualities. More importantly, the proposed method offers lower computational times—an advantage that gives more insights into the possible application of the method in time-sensitive tasks.

DECLARATION

I, Rehema H. Mwawado**,** do declare hereby to the Senate of the Nelson Mandela African Institution of Science and Technology that, this dissertation is my own original work and that it has neither been submitted nor is it being concurrently submitted for a degree award in any other institution.

Rehema Hamis Mwawado... 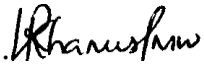 … …….

Name and signature of candidate **Date**

The above declaration is confirmed

Dr. Mussa A. Dida …… ……

Name and signature of supervisor **Date**

Dr. Baraka J. Maiseli …  ……

Name and signature of supervisor **Date**

COPYRIGHT

CERTIFICATION

The undersigned certifies that he/she has read and hereby recommend for acceptance by the Nelson Mandela African Institution of Science and Technology a dissertation titled, "Development of a Fast and Accurate Method for the Segmentation of Diabetic Foot Ulcer Images, in fulfillment of the requirements for the degree of Masters in Information and Communication Science and Engineering of the Nelson Mandela African Institution of Science and Technology."

…… …….

Dr. Mussa A. Dida Date

Supervisor

…… …….

Dr. Baraka J. Baiseli Date

Supervisor

ACKNOWLEDGEMENT

Completing this study successfully was made possible by several parties through their dedicated efforts, support and guidance.

Foremost, I thank God for granting me knowledge, ability, and opportunity of not only undertaking this research study but also persevering and completing it satisfactorily.

I would like to thank the African Development Bank (AfDB) for providing me the funds that supported this work financially.

I also gratefully acknowledge my supervisors Dr. Baraka Maiseli and Dr. Mussa Ally Dida who not only introduced me to the topic but also provided their support throughout this study. Their engagement, remarks, and comments have been invaluable.

My deep appreciation goes out to all the lecturers for their help and support. I also take this opportunity to thank my fellow classmates for the classwork we did together and for their valuable inputs in this dissertation.

Lastly I appreciate all the help and guidance I received from my parents, siblings, and friends. Thank you very much.

TABLE OF CONTENTS

LIST OF TABLES

LIST OF FIGURES

LIST OF APPENDICES

LIST OF ABBREVIATIONS AND SYMBOLS

ACRONYM	DEFINITION
CT	Computer Tomography
DFUs	Diabetic Foot Ulcers
FN	False Negative
FP	False Positive
IDF	International Diabetes Federation
MCC	Matthew Correlation Coefficient
MRI	Magnetic Resonance Imaging
MSSIM	Mean Structural Similarity
NCDs	Non Communicable Diseases
PM	Perona-Malik
PSNR	Peak Signal to Noise Ratio
ROI	Region of Interest
TN	True Negative
TP	True Positive
TV	Total Variation

CHAPTER ONE

INTRODUCTION

1.1 Background of the Problem

Diabetes Mellitus also referred to as diabetes results from high blood sugar levels over a prolonged period. In 2017, approximately 451 million people had this long term condition as estimated by the International Diabetes Federation (IDF) (Cho *et al.*, 2018). Statistics further highlight the prevalence of diabetes affecting 9.3% of the world's adult population in 2019 with almost 80% of the affected population being people from developing countries (Saeedi *et al.*, 2019). This life-long condition is often characterized by possible life-threatening complications that are associated with the disease including cardiovascular disorders, kidney failure, blindness and diabetic foot ulcers which may later result in lower-limb amputation (Patterson *et al.*, 2019).

From the aforementioned complications, Diabetic Foot Ulcers (DFUs) are the most significant, contributing to about 70% of the leg amputations (Chiwanga & Njelekela, 2015). Statistics further portray that the problem is more significant in developing countries like Tanzania since resources in terms of specialists and facilities are limited and most of the patients, are admitted to the clinics when the ulcers have fully advanced (Chalya *et al.*, 2011). Being a serious health concern for diabetic patients, successful clinical management that involves early detection and effective preventive care of the DFUs will significantly reduce comorbidities and thus in the long run improve the quality of life for the patients.

To achieve maximum accuracy thorough and critical evaluation of the ulcer should be done for proper management. This evaluation should include an efficient and sufficient description of ulcer characteristics, such as size, ulcer depth, appearance in texture as well as the location on the foot to ensure proper assessment of the progress during treatment (Mavrogenis *et al.*, 2018). To enhance the accuracy in evaluation with the aim of improving diabetic foot ulcer healing and prevention of lower limb amputation, imaging and non-invasive tests are essential. Since early ulcer diagnosis has proven to be laborious using existing dermatological practices, non-invasive ulcer assessment is possible by using digital images (Kumar & Malathy, 2016). Thus this study aims at developing a computationally fast yet accurate method for the segmentation of diabetic foot ulcers using digital image processing techniques.

In essence, this work proposes a diabetic foot ulcer image segmentation method that incorporates a hybrid diffusion-steered functional derived from the Total variation and the Perona-Malik diffusivities to detect the ulcer edges. This method employs edges as they depict local and significant intensity changes in the captured foot ulcer image. The proposed method is then evaluated in terms of the ability to produce visually appealing segmented images, robustness to noise and computational efficiency. The proposed work has following significant merits: (a) avoids complex and exhaustive geometric and mathematical modeling; (b) robustness to noise (c) guaranteeing high segmentation accuracy; (d) computationally efficient for it to be implemented in actual hardware.

1.2 Statement of the Problem

In the current practices, clinicians perform a visual examination to assess the ulcers manually using standardized scales and indices. In essence, evaluation of diabetic foot ulcers consists of various important procedures: (a) evaluating the patients' medical history; (b) thorough examination of the foot ulcer by a specialist; (c) initiation of additional tests that involve sophisticated imaging modalities such as the x-rays (Goyal *et al.*, 2017). Visual assessment is very subjective and inaccurately determines the ulcer area as well as leads to incorrect classification of the ulcer tissues (Wang *et al.*, 2015). Furthermore, the image modalities such as x-ray imaging and Magnetic Resonance Imaging (MRI) are expensive and thus not easily available in most developing countries with limited health facilities.

In the existing literature, different approaches have been implemented to address the issues of inaccuracy. Recent studies such as that done by Wang *et al.* (2019) employed an associative hierarchical random field framework to determine the boundary of the foot ulcer. Although such methods have increased accuracy they tend to suffer from the instability of unsupervised super-pixel segmentation algorithms especially with respect to the ability in recognizing objects with complicated boundaries such as the foot ulcers (Wang *et al.*, 2019). In further standardizing the accuracy of chronic ulcer assessment using computer-aided methods Fauzi *et al.* (2015) employed a method that first determines the Red-Yellow-Black-White (RYKW) probability map, then guides the segmentation process using either optimal thresholding or region growing.

Although the probability method achieves an average accuracy of 75.1%, it underperforms when segmenting and characterizing ulcers on dark skins, especially when trying to identify eschar tissues or dark granulation tissues during the segmentation process. More approaches have thus employed the level set algorithms which experience drawbacks such as complex parameter modeling, underperformance for noisy images and high computational cost (Wang *et al.*, 2015). The level set algorithms oblige one to train many parameters hence making the method computationally slower in operation (Wang *et al.*, 2013). Inspired by the weaknesses of these existing methods in literature and by the already mentioned challenges of the clinical methods in practice, a need to establish imaging methods that can objectify and increase the accuracy of the traditional methods of analyzing diabetic foot ulcers is thus necessary (Netten *et al.*, 2017).

1.3 Rationale of the Study

Biomedical image processing has experienced dramatic expansion, and has been an interdisciplinary research field attracting expertise from applied mathematics, computer sciences, engineering, statistics and medicine. Computer-aided diagnostic processing has thus become an important part of clinical routine as a means in which images can be enhanced manipulated and analyzed. Image processing studies strive to provide solutions for costly invasive assessment therapies and the less effective non-invasive therapies (Davis *et al.*, 2018). As the preliminary diagnosis of diabetic foot ulcers is relatively challenging using the existing conventional dermatological methods, scholars have recently proposed (non-invasive) image processing techniques that have demonstrated promising results. These non-contact imaging methods assist clinicians to follow the prognosis and the healing status of the ulcers without compromising the sterilization techniques required to manage such ulcers (Shah *et al.*, 2019).

1.4 Research Objectives

1.4.1 General Objective

To develop a fast and accurate method for the segmentation of diabetic foot ulcer images that becomes the basis of future computer-aided ulcer assessment techniques.

1.4.2 Specific Objectives

This research is carried out under the following specific objectives:

(i) To identify the diabetic foot ulcer image segmentation requirements
(ii) To develop an edge detector method for segmentation of diabetic foot ulcers images
(iii) To validate the performance of the proposed segmentation method

1.5 Research Questions

The research answers the following questions:

(i) What are the requirements for the segmentation of diabetic foot ulcer images?
(ii) How can a fast yet accurate segmentation method of diabetic foot ulcer images be developed?
(iii) How can the performance of the proposed method be validated?

1.6 Significance of the Study

Digital image processing offers a potential and cost-effective solution to address issues of the inaccuracy of the visual assessment as well as minimizing consecutive patient visits to the clinic. Thus the proposed image segmentation method is meant to be implemented as a computer algorithm that will be the basis of future development of software tools that will improve the accuracy of visual assessment methods and also be less expensive in terms of computational power and cost when compared to other imaging modalities like CT scans and X rays that are currently being used. This developed segmentation method is not meant to provide means of eliminating the role of the specialist but it will be a means of which will offer assistance to the specialist when accurately analyzing the DFUs. With improvement, this method can be integrated into the hardware of existing methods.

1.7 Delineation of the Study

This study involves only colored images (RGB color model) and not any other type of image. Furthermore, for images with dimensions smaller than 107x154 pixels, the method tends to underperform hence producing less accurate results.

CHAPTER TWO

LITERATURE REVIEW

2.1 Global Diabetes Prevalence and it's Complications

Diabetes is a significant public health problem one of the four priority non-communicable diseases (NCDs) listed in the sustainable development goals and is targeted for action (Bennett *et al.*, 2018). Both the number of cases and the prevalence of diabetes has been steadily increasing over the past few decades. As a global burden, an estimated 422 million adults were living with diabetes in 2014 compared to 108 million in 1980. Diabetes leads to life-threatening complications in many parts of the body and can increase the overall risk of premature death. Possible complications include heart attack, stroke, kidney failure, vision loss, nerve damage and leg amputation that is often preceded by foot ulceration.

Foot ulceration occurs in as many as 15–25% for both type 1 and 2 diabetic patients over their lifetimes (Nouvong *et al.*, 2009). The burden of diabetic foot disease is set to increase in the future since the contributory factors to foot diseases such as peripheral neuropathy and vascular disease are present in more than 10% of people at the time of diagnosis of the disease (Boulton *et al.*, 2005). To address the issue of ulceration management, this study thus focuses on image segmentation of foot ulcers from digital images.

2.2 Digital Image Processing

Over the years, diagnostic imaging has become an invaluable tool in the field of medicine. The most commonly used imaging modalities including but not limited to magnetic resonance imaging (MRI), computed tomography (CT) and digital mammography. These aforementioned imaging modalities provide an effective means for non-invasively mapping the anatomy of a subject. As of recent, these technologies have greatly increased knowledge of normal and diseased anatomy for medical research and are a critical component in diagnosis and treatment management (Kobayashi *et al.*, 2010).

During the last couple of years, digital image processing has been widely used in medicine, biology, physics and engineering. It is a type of signal processing whose input is an image and output may be an image or characteristics/features associated with that image. An image is defined as a two-dimensional function $f(x, y)$, where x and y are spatial (plane) coordinates

and the amplitude of $f(x, y)$ at any pair of coordinates (x, y) is called the intensity or gray level of the image at that point. When x, y, and the intensity values of f are all finite discrete quantities, it is then referred to as a digital image (Tyagi, 2018).

The growing size and number of digital medical images have necessitated the use of computers and other digital mobile devices to facilitate their processing and analysis. In particular, computer algorithms for the delineation of anatomical structures and other regions of interest are becoming increasingly important in assisting and automating specific radiological tasks (Pham *et al.*, 2000). These algorithms, called image segmentation algorithms, play a vital role in numerous biomedical-imaging applications such as the quantification of tissue volumes, studying of anatomical structures, diagnosis and localization of pathologies.

The prior goal of any image segmentation method is to make things simpler and transform the representation of images into a meaningful subject. Image segmentation can either be automatic or semiautomatic. One of the challenging problems is segmenting the regions with missing edges, absence of texture contrast, the region of interest (ROI) and background (Varshney *et al.*, 2009).Thus to accurately segment the foot ulcers this study focuses on first identifying the edges of the ulcer on a particular image by proposing a new edge detector method then getting the region of interest which is the ulcer area. To understand both the edge detection techniques and the grounds used to propose the new segmentation method, a detailed review of the edge detection methods used in many works of literature, as well as an overview of the segmentation methods, are explained in the next subsections.

2.2.1 Edge Detection

Edge detection is one of the fundamental steps in image analysis and is useful in finding the key features in images. In digital images, edges are used to depict local and significant intensity changes. Edges are local discontinuities or abrupt changes in image grey values and/or texture. The main purpose of edge detection is to simplify the image data in order to minimize the amount of data to be processed. Thus edge detection has become an important part of the pre-processing stage before the segmentation or classification of medical images and thus plays a vital role in medical image analysis (Muthukrishnan & Radha, 2011).

Conventionally, edges are detected using Sobel, Prewitt or Laplacian of Gaussian operators. In theory, these operators belong to high pass filtering, which is not quite suitable for edge

detection in most medical images due to the fact that noise and edges belong to the same scope of high frequency. Furthermore, these edge detectors are based on detecting points in the image with a high image gradient value. Due to this, many other edge points are detected, but some of them do not really belong to an edge that qualifies to be in the intended output (Sharma *et al.*, 2012).

Comparative evaluation of edge detectors facilitates the process of deciding an appropriate method for the segmentation of diabetic foot ulcers in the digital image. For this purpose, two main approaches have been proposed in the literature as shown in Fig. 1. The gradient-based approaches, which detect the edges by finding maximum and minimum values of the image's first derivative and the Laplacian-based approaches, which search for zero crossings in the image's second derivative. The approaches are thus known as classical methods (Maini, 2009). In addition to these classical techniques, researchers have also employed diffusion-based and total variation (TV) methods to locate potential image features. The motivation for extending the research to such methods is inspired by the weaknesses of the aforementioned classical methods (Bayraktar *et al.*, 2019). Both the classical methods and the diffusion-based methods are discussed in the next subsections.

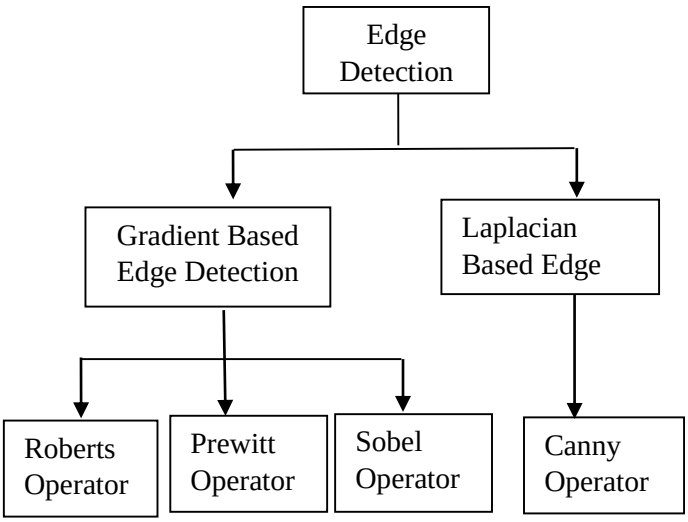

Figure 1: Classical Edge Detection Techniques (Maini, 2009)

(i) Roberts cross operator

This edge detector computes a 2-D spatial gradient measurement on an image. It highlights the regions that have a high rate of change of the image intensity values in the spatial domain of the image under test. These regions with a high spatial frequency normally correspond to edges. Pixel values at each point in the output image represent the estimated absolute magnitude of the spatial gradient of the input image at that point (Berbar *et al.*, 2006).

In theory, the Roberts cross operator consists of a pair 2x2 convolution kernel whereby one of the kernels is a 90° rotation of the other as shown in Fig. 2. These kernels are designed in such a way that they maximally respond to edges that are 45° to the pixel (Subhro & Ardhendu, 2015). To get the corresponding edge map these kernels can be applied separately to the input image so that they produce separate measurements of the gradient component in each orientation. These measurements are then combined together to find the absolute magnitude of the gradient at each point and the orientation of that gradient.

+1	0
0	-1

(a)

0	+1
-1	0

(b)

(a) horizontal mask, (b) vertical mask

Figure 2: Roberts Edge Detector Masks (Subhro & Ardhendu, 2015)

Despite its simplicity and less computational requirements, this operator suffers from two main drawbacks. Foremost, it is very sensitive to noise due to the use of a very small kernel. Secondly, the gradient magnitude of the edges also degrades with the increase in noise which in return produces inaccurate results. Furthermore, it produces very weak responses to genuine edges unless they are very sharp (Chandwadkar *et al.*, 2013).

(i) Sobel operator

Sobel edge detection is achieved by implementing a 2D spatial gradient convolution operation on a digital image. The Sobel edge detector computes the gradient by getting the discrete differences between rows and columns of a 3X3 neighborhood (Asmaidi *et al.*, 2019). It employs a pair of 3X3 convolution masks, where one estimates gradient in the x-direction and the other estimates gradient in the y-direction as shown in Fig. 3.

-1	0	1
-2	0	2
-1	0	1

(a)

1	2	1
0	0	0
-1	-2	-1

(b)

(a) horizontal mask, (b) vertical mask

Figure 3: Sobel Edge Detector Masks (Asmaidi *et al.*, 2019)

These kernels are designed to respond maximally to edges running vertically and horizontally relative to the pixel grid. Like the Roberts cross operator, the kernels can also be applied separately to the input image, such that they produce separate measurements of the gradient component in each of the corresponding orientation. The large convolution kernels of the Sobel operator smooth out the input image to a greater extent and hence makes the operator less sensitive to noise. Thus this operator generally produces considerably higher output values for similar edges, compared with the Roberts Cross operator (Shrivakshan, 2012).

In spite of the promising output results, the Sobel operator is slower in operation and like the Roberts operator, it can also overflow the maximum allowable pixel value for an image type that supports small integer values like 8-bit integer images (Vincent & Folorunso, 2009). Thus to accurately employ this operator one has to use image types with larger pixel ranges. Furthermore, the smoothing effect of the Sobel operator often leads to lines in the output image that are several pixels wide thus some thinning techniques may be desirable.

(ii) Prewitt operator

The Prewitt operator masks are shown in Fig. 4. This operator detects both horizontal and vertical edges. The masks work as a first-order derivate which calculates the difference of pixel intensities in an edge region. The vertical mask consists of zeros in its center column, hence it does not include the original values of an image but rather it calculates the difference of right and left pixel values around that edge.

-1	0	1
-1	0	1
-1	0	1

(a)

1	1	1
0	0	0
-1	-1	-1

(b)

(a) horizontal mask, (b) vertical mask

Figure 4: Prewitt Edge Detector Masks (Tian, 2012)

The horizontal mask consists of zeros in its center row so it does not include the original values

of the edge in the image but rather it calculates the difference of above and below pixel intensities of the particular edge (Ferhat *et al.*, 2013). Since the Prewitt edge operator only has two templates with horizontal and vertical directions it cannot locate the edges in all other directions (Yang *et al.*, 2011).

(iii) Canny edge detector

The Canny edge detection method is widely recognized to be the standard edge detection method in the image processing industry. It is a multistage edge detection algorithm with a sequence of operations. It includes steps of preprocessing using a Gaussian filter, calculation of gradients, suppression of all the non-maximum pixels and lastly performing a threshold with hysteresis (Nagaraju, 2017). Figure 5 shows a 3x3 mask of the canny edge detector.

-1	0	1
-2	0	2
-1	0	1

(a)

-1	-2	-1
0	0	0
1	2	1

(b)

(a) horizontal mask, (b) vertical mask

Figure 5: Canny Edge Detector Masks

The two key parameters of the canny edge detection are the upper and lower thresholds. The upper threshold marks edges that are the actual edges whereas the lower threshold finds faint pixels that are also part of an edge. In practice, the upper tracking threshold can be set quite high, and the lower threshold quite low for good results. The upper threshold should be set such that it does not increase the number of spurious and undesirable edge fragments appearing in the output (Nagaraju, 2017).

The performance of the canny operator is determined by three parameters: The width of the Gaussian kernel used in the smoothing phase, and the upper and lower thresholds used by the tracker. Increasing the width of the Gaussian kernel reduces the detector's sensitivity to noise, at the expense of losing some of the finer detail in the image. The localization error in the detected edges also increases slightly as the Gaussian width is increased (Luo *et al.*, 2017). The canny operator produces superior output results compared to Roberts and Sobel operators however one major problem with the basic canny operator is it tends to underperform when an edge to be detected is partially occluded by another object (Feng *et al.*, 2017).

(iv) Laplacian of Gaussian

The Laplacian of Gaussian is a 2-D isotropic measure of the second spatial derivative of an image (Shahnoor & Khan, 2012). A Laplace operator may detect edges as well as noise (isolated, out-of-range). Thus to obtain the desired output from this detector, the input image is first smoothed using a Gaussian kernel. The input image is represented as a set of discrete pixels, hence to approximate the second derivative in the definition of the Laplacian a discrete convolution kernel is used. Three commonly used small kernels as discussed by Assirati *et al.* (2014) are shown below in Fig. 6.

0	1	0
1	-4	1
0	1	0

1	1	1
1	-8	1
1	1	1

-1	2	-1
2	-4	2
-1	2	-1

Figure 6: Laplacian Filter Approximations (Assirati *et al.*, 2014)

2.2.2 Anisotropic Diffusion

Foremost, diffusion with regards to image processing is modeled as an image restoration or smoothing problem (Morfu, 2010). Palma *et al.* (2014) interpreted an image as the initial concentration distribution with high and low pixel intensities as illustrated in the equation as:

$$u(x, y, t = 0) = I(x, y) \tag{2.1}$$

In essence, diffusion involves the process where low-value pixels receive weight from high-value ones without modifying the total pixel count (Palma *et al.*, 2014). The diffusion concept in images can either be isotropic or anisotropic depending on how it is applied in a particular application. In isotropic diffusion, the smoothing (diffusion) of the pixel value takes place all across the image which results in blurring of edges. Anisotropic diffusion, on the other hand, is carried out depending on the image edges and their direction.

Over the years, anisotropic diffusion has attained a lot of attention for image restoration and smoothing tasks. The first formulation of anisotropic diffusion was broached by Perona and Malik (1990). They developed an adaptable smoothing and edge detection scheme in which the linear heat diffusion equation is replaced by a selective diffusion that preserves the edges.

The Perona-Malik model makes use of anisotropic diffusion to filter out the noise and enhance the output image. The PM model aims to reduce image noise without removing significant parts of the image content, typically edges, lines or other details that are important for the interpretation of the image (Kessy *et al.*, 2017). In the PM model, the rate of diffusion is controlled by an edge stopping function which possesses a high image gradient. Based on this gradient value smoothing is performed. If the magnitude of the gradient is small then smoothing is done otherwise it is stopped. Since edges are the regions with large gradients from the PM a backward diffusion in the gradient direction leads to sharpening of the edges instead of blurring them. The PM model, however, experiences the following setbacks which limit its implementation.

(i) Tends to add speckles into evolving solutions (Guo *et al.*, 2012).
(ii) It suffers from stair-casing problems and its corresponding energy potential is non-convex hence it is prone to instabilities and multiple solutions (Guidotti, 2012).
(iii) Works well for images affected with additive noise (Gupta *et al.*, 2016).

2.2.3 Total Variation

In recent years, the total variation (TV) method has attracted researchers such that it has been included in many works of literature. The TV model also termed as total variation regularization generates appealing results for both objective and subjective qualities. To understand the significance of TV in preserving edges we review the total variation minimization pioneer model proposed by Rudin *et al.* (1992). Also termed as ROF, this total variation model employs an approach for noise reduction developed to preserve sharp edges in the underlying image signal. Unlike a conventional low-pass filter, TV denoising is defined in terms of an optimization problem. The output of the TV denoising 'filter' is obtained by minimizing a particular cost function (Selesnick, 2012).

In real-world applications, the observed image f represents a noisy version of a true image u that is characterized by homogeneous regions, and sharp edges. The noise or small scale repeated details can be represented as. In the presence of the additive noise, the relation between f and u can be expressed by the linear model as:

$$f(u) = u(x, y) + v(x, y) \tag{2.2}$$

In this ROF model, the problem of reconstructing u from f is posed as a minimization problem in the space of functions of bounded variation, allowing edges or discontinuities along curves. Their model, very efficient for denoising images while keeping sharp edges is given as:

$$\inf_{u \in L^2} F(u) = \int |\nabla u| + \lambda \int |f - u|^2 \, dx \, dy \,, \tag{2.3}$$

Where $\lambda > 0$ is a tuning parameter. The second term in the energy is a fidelity term, while the first term is a regularizing term, to remove noise or small details while keeping important features and sharp edges (Yan & Shu-Ling, 2013).

Although this model can preserve important features of the image such as edges, it tends to experience the following setbacks.

(i) It results in the creation of lease edges on the image (Tang & Fang, 2016).
(ii) It reduces the contrast of an image.
(iii) Total variation is affected by blocky artifacts.
(iv) Images resulting from this algorithm are piecewise constant implying that some of the features cannot be fully recovered and creates the staircase effects on the image (Zeng, 2015).

2.2.4 Image Segmentation

As stated in the previous sections, image segmentation is an integral component in digital image processing. It divides the image into different segments and discrete regions. Most of the segmentation algorithms are based on one of two basic properties of image intensity values which are discontinuity and similarity. In the first category, the approach is to partition an image into regions based on abrupt changes in intensity, such as edges. Approaches in the second category are based on partitioning an image into regions that are similar according to a set of predefined criteria. Thresholding, region growing and region splitting are some vivid examples of the second approach (Kaur & Kaur, 2014).

Several of these approaches have appeared in the recent medical image segmentation related literature. For the purpose of this research, the methods that are relevant to this study are defined, provide an overview of the implementation, and discuss the related merits and most notable drawbacks associated with the particular methods. It should be noted that although each

technique is described separately, in practice multiple techniques are often used in conjunction in solving different segmentation problems to achieve more accurate results.

(i) Region Growing and Merging

Region merging works by building up complicated regions in a manner that combines smaller regions based on a statistical similarity test. This building up process in region growing can be also be considered a special case of region merging. This technique extracts an image region that is connected based on some predefined criteria. The choice of the criteria is mostly based on intensity information and/ or image edges. The region growing requires a manually selected seed point that extracts all pixels connected to the initial seed based on the already mentioned predefined criteria (Peng *et al.*, 2010). Region growing is seldom used alone as it can rarely be proven to converge to the minimum of some global cost function, and the resulting regions may have noisy boundaries (Pratondo *et al.*, 2014). Region growing find most of its applications in the delineation of small lesions and tumors.

(ii) Deformable Models

This section surveys deformable models, a promising and vigorously researched model-based approach to computer-aided medical image analysis. The widely recognized efficacy of these deformable models stems from their ability to not only segment and match but also track the region of interest by exploiting both the constraints derived from the image data together with prior knowledge about the location, size, and shape of these structures (Olveres *et al.*, 2017). To delineate an object boundary in an image, a closed curve must first be placed near the desired boundary and thereafter the curve is initialized and allowed to undergo an iterative relaxation process. Computation of the internal forces is done from within the curve or surface to keep it smooth as it deforms. On the other hand, deriving the external forces is usually from the image itself in a way that drives the curve or surface toward the desired feature of interest.

2.3 Related Works

Over the years, substantial work has been devoted to developing key telemedicine systems to monitor diabetes and its related complications. These systems employ different computer vision tasks as a means of offering cost-effective solutions for remote detection, analysis and prevention of DFUs (Goyal *et al.*, 2019). The computer vision tasks use different image processing and deep learning algorithms to analyze medical images from various modalities

such as MRI, CT scan, X-ray, and ultrasound (Yap *et al.*, 2018). These studies that employ these computerized methods have gained popularity as they strive to be a solution for costly invasive assessment therapies and the less effective non-invasive therapies which involve either measuring width and lengths of the wound with a ruler and then applying a formula that assumes elliptical shape to the ulcer or placing a sterile transparent sheet on the ulcer and tracing it (Davis *et al.*, 2018).

However, there are very few intelligent systems developed for the assessment of diabetic foot pathologies as most of these systems are based on classification tasks for the detection of abnormalities on the digital medical images (Goyal *et al.*, 2017). As these systems are mostly based on classification tasks, studies that first segment the ulcer from the rest of the background are thus crucial. A number of studies have therefore been carried out to help in the accurate diagnosis of the foot ulcers as well as presenting computerized tools to assist dermatologists in the segmentation of skin lesions in localized clinical images. In literature, these computerized approaches employ various edge detectors as part of their pre-processing stages. Most notable examples include the work done by Fraiwan *et al.* (2017) where they employed the Sobel operator to exclude the edges of the feet in the developed thermal imaging system for the foot ulcers. In their work, the main focus was to get the feet edges and not the particular ulcer area. As this method was fully dependent on the temperature gradient from the acquired thermal images, it tended to generate false positives around the ulcer area.

Another technique that was proposed based on a radial search method to segment the ulcers. This method serves the purpose of true border extraction in the domain of relevant to skin images affected by wounds. The radial search method is semiautomatic and thus needs manual initialization of search origin (Kumar & Malathy, 2016). The evolution methods completely depend on the initial curve which has to be pre-delineated either manually or by a well-designed algorithm (Wang *et al.*, 2015). Another approach to increase the segmentation accuracy employed an asymmetric analysis that could detect diabetic foot complications by comparing the two feet of the patient (Liu *et al.*, 2015). However this method underperforms when one of the foot is amputated.

Liu *et al.* (2013) on the other hand used an edge detection method that is based on active contour models (ACMs) as an attempt to address the drawbacks of conventional methods. Although the ACMs have superior sub-pixel accuracies as compared to the conventional

methods, their outputs can be easily affected by the intrinsic disadvantages of the active contour algorithms, including contour's initial position and noises in the images. Other prominent previous segmentation methods include the level set method to determine the wound boundary (Wang *et al.*, 2013). In these formulations, the level set function typically develops irregularities during its evolution, which may cause numerical errors and eventually destroy the stability of the evolution.

CHAPTER THREE

MATERIALS AND METHODS

3.1 Study Design

This study follows a descriptive study design, where the physical features of diabetic foot ulcers are observed and photographed. The digital images taken were used to build a diverse data set for the purpose of this study. The study involved only diabetic patients with at least one foot ulcer that were admitted or attended the diabetic clinic within Tanzania. The diabetic clinics in Tanzania were chosen at random.

3.1.1 Inclusion Criteria

Patients aged 21–85 years diagnosed with type 1 or type 2 diabetes with at least one DFU were eligible. The age group was chosen as most of the amputation cases that are preceded by DFUs are prevalent in this group of individuals (Al-rubeaan *et al.*, 2015). The diagnosis of type 1 and type 2 diabetes was established by a specialist. This study included both men and women attending a diabetic clinic and have consented to participate in the study.

3.1.2 Exclusion Criteria

The study excluded patients that were admitted or attended the diabetic clinic due to other complications of the disease but had no diabetic foot ulcers. It also excludes the patients who had ulcers but did not consent to participate in the study.

3.2 Data Collection

A dataset was built using images from public domains and various diabetic clinics in Tanzania. Permission was granted to use the freely available diabetic foot ulcer images from accredited sources. The approach of using internet images allows universal evaluation of the proposed method against the existing classical approaches. To ensure diversity in the dataset, ethically consented diabetic foot ulcer images from patients in the selected diabetic clinics were also used for this study. The diversity in this context refers to heterogeneity in the dataset with regards to varieties in skin type due to ethnicity as well as angles that the images are taken from and the separating distance between the camera and the diabetic foot ulcer. The study was then performed following a uniformed study protocol that was approved by the institutional review

boards at each center. After receiving a description of the protocol and asking questions, all patients agreeing to participate signed an approved informed consent form.

3.2.1 Ethical Considerations

Ethical clearance was sought from the Northern Tanzania Health Research Ethics committee. Informed consent was also sought from all patients and signed for those willing to participate. Permission to conduct this study within the Arusha region in Tanzania was sought from the Regional Commissioner's office and other relevant offices.

3.3 Research Framework

Intuitively, image segmentation is the process of dividing an image into different regions such that each region is homogeneous while not the union of any two adjacent regions. For this study, an edge detection method is first developed. It is then used in the pre-processing stage before the segmentation is done. As part of the post-processing stages, morphological operations are applied to accurately get the region of interest. The research framework is as shown in Fig. 7.

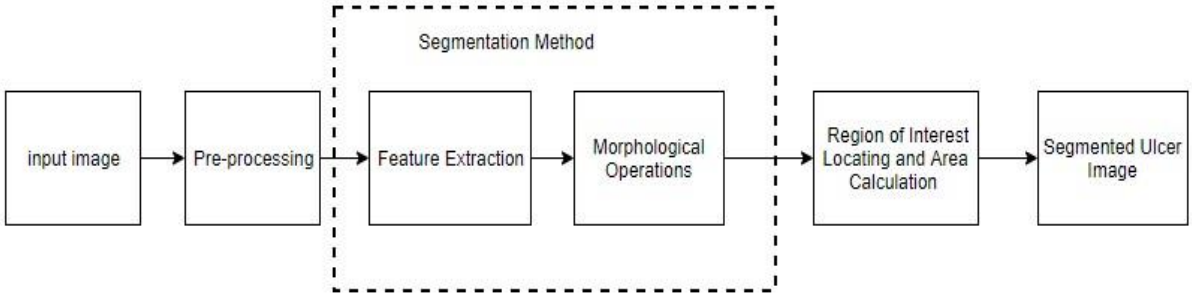

Figure 7: Research Framework

3.4 Requirements

To set up the environment to develop the proposed method this study first identifies the software and hardware requirements that can be used. The software requirements give an interactive set of instructions to develop the method whereas the hardware requirements include the physical environment in which the method will run and be stored.

3.4.1 Software Requirements

Windows 10 operating system was used during the development process. For the image processing, part MATLAB environment was used. MATLAB provides an interactive environment with several built-in functions that are appropriate for the development of the method. The used software tools, their versions, and sources are given in Table 1.

Table 1: Software Tools, Versions, and Sources

Software Product Name	Version	Source
Microsoft Windows 10 Home	10.0.17134 Build 17134	https://www.microsoft.com/
MATLAB R2018a	MATLAB 9.4	https://www.mathworks.com/

3.4.2 Hardware Requirements

Computational power is a very important aspect when processing digital images. Each component of a typical computer configuration listed below has an impact on the MATLAB performance and thus will directly affect the performance of the method developed.

(i) Central Processing Unit (CPU)

Computers with more CPU cores can outperform those with a lower core count, but results will vary with the MATLAB application. To enhance the performance of the segmentation method, the development and testing were done using a computer with Intel or AMD x86-64 processor with four logical cores and AVX2 instruction set support.

(ii) Memory

A minimum of 4GB RAM is recommended to prevent performance degradation due to thrashing when MATLAB and other programs are running concurrently with it. For the development and testing of the method 16GB RAM was used.

(iii) Hard disk

The hard disk speed is a significant factor in the MATLAB start-up time. A full installation of all MathWorks products that were used in the development and testing of the proposed method takes up to 23 GB of disk space. Thus a computer with a hard disk of 1TB was used in this study.

3.5 Developing the Edge Detection Method

(i) Combining the Total variation and Perona-Malik diffusivities

Inspired by the weaknesses of the mentioned traditional methods, an alternative approach is proposed to facilitate the segmentation of a diabetic foot ulcer from an image, u. Let u_x and u_y be the horizontal and vertical derivatives of u, respectively. Furthermore, because an edge denotes a significant local change in the image intensity, it is usually associated with a discontinuity in either the image intensity or in the first derivative of the image intensity. The change in intensity level is measured by the gradient of the image. The diabetic foot ulcer image $u(x, y)$ is a two-dimensional function hence its gradient is a vector. The magnitude and the direction of the gradient are respectively computed as:

$$|\nabla u| = \sqrt{{u_x}^2 + {u_y}^2} \tag{3.1}$$

$$\alpha(x, y) = \tan^{-1}\left[\frac{u_y}{u_x}\right] \tag{3.2}$$

Figure 8 illustrates the general structure of the proposed edge detection method. The proposed technique will be discussed in detail in the next subsections. From the illustration, the diabetic foot ulcer image u is converted into a grayscale image. The use of the grayscale image simplifies the algorithm and reduces computational requirements. The MATLAB command *im2double* is used to convert the grayscale diabetic foot ulcer image to double precision and rescaling the data if necessary. Thus the equation below gives the new edge detector used to find the edges of a 2-dimensional diabetic foot ulcer image as:

$$E(|\nabla u|) = \frac{1}{1 + \frac{|\nabla u|}{k_1} + \left(\frac{|\nabla u|}{k_2}\right)^2} \tag{3.3}$$

Where $k_1 > 0$ and $k_2 > 0$ denote the tuning constants that determine a tradeoff between clarity of edges and noise. Considering the denominator of the proposed functional, the second and third terms from left signify versions of the Total Variation and the Perona-Malik methods. The proposed functional ensures that a proper balance is established between weaknesses and strengths of the two formulations, as evidenced by clearer and stronger edges recovered by the proposed edge detector.

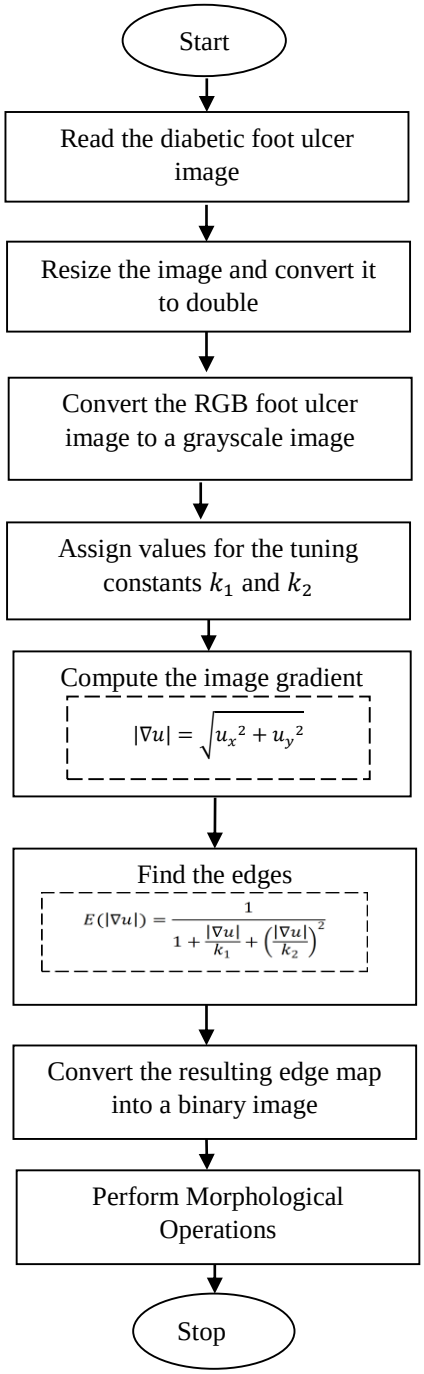

Figure 8: Proposed Edge Detection Method

(ii) Mathematical Morphology

To increase the accuracy of locating and connecting the edges of the ulcer area a number of morphological operations are employed. A connected object here refers to an entity in the image that is continuous and has no breaks. The MATLAB function *bwconncomp* is used to get the connected ulcer area edges from the obtained binary image of the resulting edge map. Now applying the function *regionprops* on each entity, the individual properties such as *pixelList* and pixel area can be found. The *regionprops* function returns measurements for the set of properties specified for each 8-connected object in the binary image of the edge map. Using these region properties in MATLAB all the areas that are below pixel area of 150 are eliminated. The eliminated area are short lines outside the region of interest which are due to small objects in the image, or texture areas.

The tuning constants, k_1 and k_2, control the sensitivity of the method. To ensure that the resulting edge map is clearly defined, the MATLAB skeletonization function *bwskel* was used. This function reduces all objects in the two-dimensional binary image to one-pixel curved lines without changing the essential structure of the image. The process extracts the centerline while preserving the topology of the resulting foot ulcer edge map image and the Euler number of the objects in the image.

3.6 Developing of the Overall Segmentation Method

After getting the edge map using the proposed edge detector described in section 3.5 the foot ulcer is then segmented from the background of the image. To delineate the foot ulcer region from the edge map image an active contour model is employed. The active contour model (or snakes), was first introduced by Kass *et al.* (1988).

Active contours form to the edges of the region of interest by minimizing a summation of energies. The two main energies are internal and external energy, but others like a ballooning force (Acton & Ray, 2009) can also be included. These curves are defined within an image domain and they move under the influence of internal forces within the curve itself as well as external forces derived from the image data.

A contour parameterized by arc length s is defined and illustrated in equation 3.4. This curve moves through the spatial domain of the foot ulcer image to minimize the energy functional in equation 3.5. For the purpose of this study, the internal and external forces are defined in such a way that they will compel the snake to conform within the ulcer boundary and are given by:

$$v(s) = [x(s), y(s)], s \in [0,1] \tag{3.4}$$

$$E\big(v(s)\big) = E_{int}\left(v(s)\right) + E_{ext}\left(v(s)\right) \tag{3.5}$$

Where E_{int} is the internal deformation energy that characterizes the active contour. The internal energy function determines the regularity, i.e. smooth shape, of the contour. In this study, a list of points to initialize the active contour and the internal energy is defined in a way that it minimizes an approximation of the first and second derivative of the contour. Since the list of points for the active contour is used, two scaling factors which weigh the first and second derivatives of the active contour to create the internal energy are thereafter defined. Hence, the quadratic functional given that represents the internal energy is given by:

$$E_{int} = \int_0^1 (\alpha|v'(s)|^2 + \beta|v''(s)|^2)ds \tag{3.6}$$

Where α and β are weighting parameters that control the snake's tension and rigidity, respectively, and $v'(s)$ and $v''(s)$ denote the first and second derivatives of $v(s)$ with respect to s.

The external energy function E_{ext} is derived from the image so that it takes on its smaller values at the features of interest, such as boundaries and is expressed as:

$$E_{ext} = \int_0^1 P\left(v(s)\right) ds \tag{3.7}$$

Where $P(x, y)$ denotes a scalar potential function defined in the image plane. To define the external force with an appropriate scalar potential function that will 'push' the active contour points to the ulcer region, the Marr method (Marr & Hildreth, 1980) is used. This method defines the external energy in such a way that it is minimized when the active contour sits near the edge of the ulcer is given by:

$$E_{ext}\,(x, y) = -|\nabla[G(x, y) * I(x, y)]|^2 \tag{3.8}$$

where $I(x, y)$ is the diabetic foot ulcer edge map image, $G(x, y)$ is a Gaussian blur, $*$ is the 2-D convolution operation, ∇ is the vector gradient operation, and $|\cdot|$ is the magnitude of the vector.

The Gaussian blur convolution is used since it has two major effects on the above equation. First, the Gaussian blur spreads out the sharp changes in gradient so that the active contour points that are further away from the edge will be "pulled" towards that edge. Second, if the diabetic foot ulcer image is slightly blurry, the edge can span over multiple pixels with a weaker gradient. The Gaussian blur will combine these gradients in such a way that their total energy will be near the same as a sharp edge that has a large gradient between a few pixels.

The MATLAB implementation of the segmentation method is as illustrated in Fig. 9. The diabetic foot ulcer is converted to grayscale and the resulting edge map is found using the proposed edge detector. Using the MATLAB function *roipoly* an interactive polygon tool associated with the edge map that is currently being displayed is created. The polygon defines a list of points around the region of interest i .e. the ulcer area. The mask is then initialized and it is true inside the polygon and false for the rest of the edge map image.

To get the internal and external energies that delineate the ulcer boundaries more accurately, it was found that defining the weighing constant $\alpha = 0.2$ and the maximum number of iterations as 500 gives better results. Post-processing operations are then performed using mathematical morphology such as *imclose* to get a better final segmentation mask output.

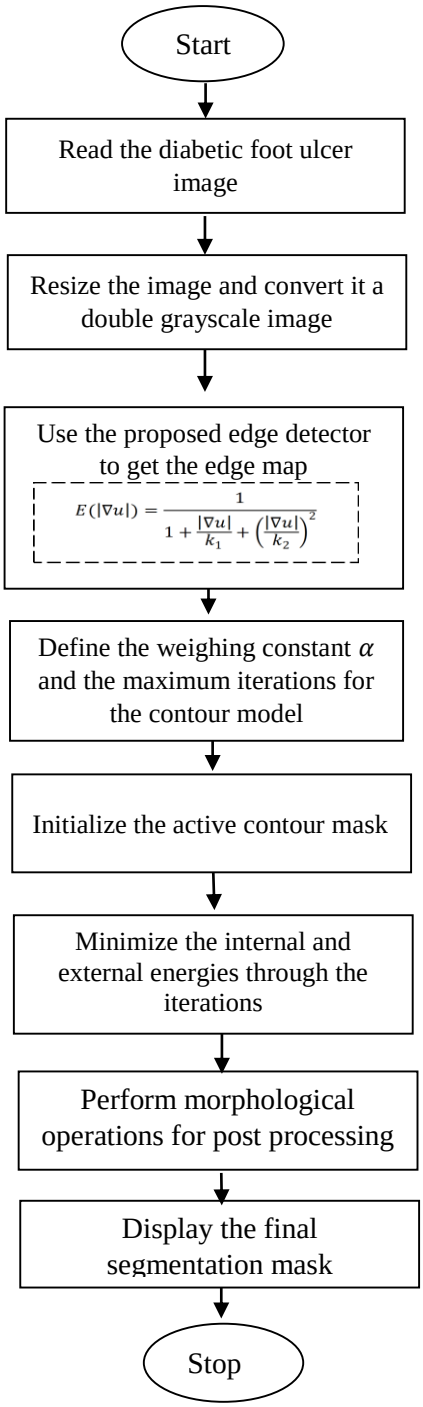

Figure 9: Workflow of the Overall Segmentation Method

3.7 Edge Detection Evaluation

As stated earlier the effectiveness of many image processing and computer vision tasks such as classification and segmentation, depends on the perfection of detecting meaningful features most importantly edges. The main objective was to develop a fast and accurate segmentation method hence developing an effective edge detector was among the objectives. To evaluate the proposed edge detector the metrics are defined and the results are then shown.

3.7.1 Edge Detection Evaluation Metrics

To decide the quality of the results from the edge detectors, the following principles have adhered: Foremost, the edge detector should accurately find all real edges (and should ignore false edges); secondly, the edges should be found in the correct image locations; and, thirdly, there should not be multiple edges found for a single edge.

(i) Visual Appeal

The ability of the detector to locate true edges and ignore all other false edges brings about the visual appeal of the final edge map output. In this research, an appealing edge map is that which highlights the ulcer area and thus clearly separating it from the rest of the background. Furthermore for the output edge map to be more appealing the edge detector should ignore all other short lines outside the region of interest that are due to small objects in the image, or texture areas.

(ii) Peak Signal to Noise Ratio (PSNR)

The Peak Signal to Noise Ratio (PSNR) measures signal strength relative to noise in the image and is defined by the equation (4.1) and is calculated decibels (dB), between the two images. This ratio is used as a measure of quality between the original and a reconstructed image. Thus PSNR can be regarded as a rough estimation of human perception of reconstruction quality. To calculate the PSNR, the mean squared error (MSE) is first calculated as;

$$\mathrm{PSNR} = 10\log_{10}\left(\frac{R^2}{\mathrm{MSE}}\right), \tag{4.1}$$

Where R is the maximal variation in the input image data. For an 8-bit unsigned integer data type, R is 255. The MSE is given by:

$$MSE = \frac{\sum_{M,N} [E(m,n) - O(m,n)]^2}{M,N} \quad (4.2)$$

where $O(m,n)$is the original image, $E(m,n)$ is the output image after the edges are detected.

The MSE is a signal fidelity measure that compares two signals by providing a quantitative score that describes the degree of similarity/fidelity or, conversely, the level of error/distortion between them. Usually, it is assumed that one of the signals is an original, while the other is distorted or contaminated by errors (Wang & Bovik, 2009).

The experiments in this work compare the output of each detector's resulting edge map of the grayscale diabetic foot ulcer images under test before and after a distortion. The distortion for this case is the addition of salt and paper noise whose noise density is 0.05.

(iii) Mean Structural Similarity (MSSIM)

Though widely applied in many image processing disciplines, PSNR fails to explain the quality of edges in the restored scenes (Maiseli *et al.*, 2015). To provide a better evaluation metric, Wang and colleagues proposed a metric (MSSIM) that explains the statistical inter-dependency of pixels in scenes, thus quantifying their visuals (Wang *et al.*, 2004).The MSSIM between *u* (restored image) and *f* (initial ideal image) is illustrated as:

$$SSIM = \frac{(2\mu_u\mu_f + c_1)(2\sigma_{uf} + c_2)}{(\mu_u{}^2 + \mu_f{}^2 + c_1)(\sigma_u{}^2 + \sigma_f{}^2 + c_2)} \quad (4.3)$$

where the variables, respectively defined for u and f are as follows: μ_u andμ_f, mean; $\sigma_u{}^2$ and $\sigma_f{}^2$, variance; andσ_{uf} , covariance; $c_1$and $c_2$are stabilizing constants.

(iv) Execution Time

To assess the computational complexity of the proposed method, the time taken for the proposed edge detector to output the corresponding edge map is evaluated. In this work the MATLAB stopwatch timer functions, *tic* and *toc* are used to compare the execution time of the classical edge detectors to that of the proposed method for each of the test images. Invoking *tic* starts the timer, and the next *toc* reads the elapsed time.

3.8 Ulcer Area Segmentation Validation

After getting the edge map the ulcer area from the rest of the background is segmented from the rest of the background. The active contours described in section 3.7 are employed. To evaluate the performance, visual appeal of the segmented output using the proposed method is compared with the outputs from the active contour without edges method proposed in by Chan Vase and the localized segmentation method proposed in (Lankton *et al.*, 2007). Various validation metrics to compare the resulting output to the ground truth image are also used.

3.8.1 Generation of Ground Truth Data

To quantitatively validate the developed segmentation method, the MATLAB segmentation app was used to generate the ground truth images by delineating the ulcer boundaries. These delineations were based on the manually traced boundaries suggested by an experienced clinician. The ground truth in this context is the ulcer area in the manual annotation that has maximum overlap with that segmented object. The generation of the ground truth image is as shown in Fig. 10. The resulting binary ground truth image that is then exported to the MATLAB workspace is shown in Fig. 11.

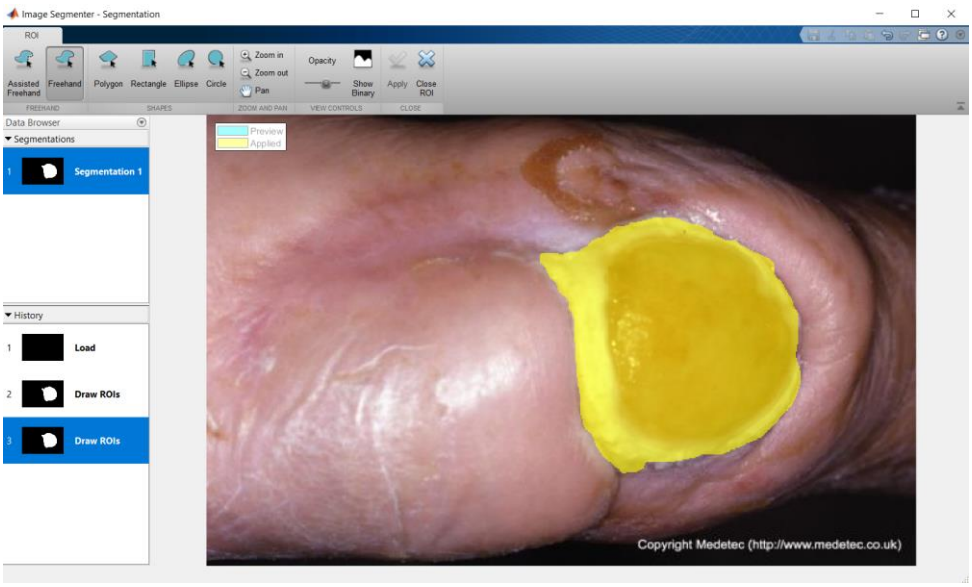

Figure 10: Delineations of the Ulcer Boundaries

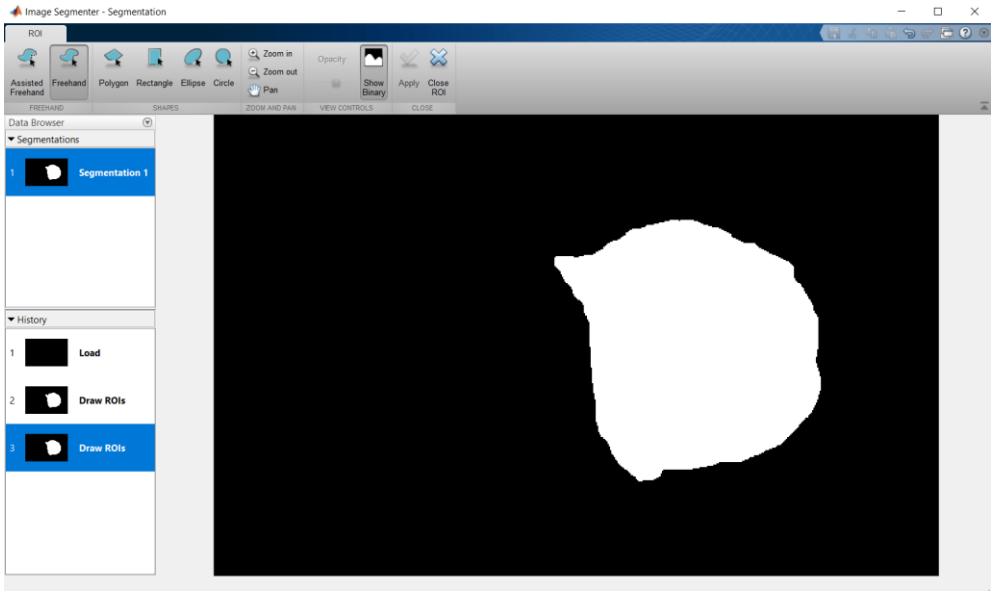

Figure 11: Resulting Binary Ground Truth Image

3.8.2 Segmentation Validation Metrics

To objectively validate the segmentation method the following metrics were employed; pixel accuracy Dice similarity, Intersection-Over-Union (Jaccard Index) and Matthew Correlation Coefficient (MCC). These metrics test how similar the output is to the ground truth as well as how correct is the method when locating the ulcer boundary.

(i) Pixel Accuracy

Pixel accuracy is the percent of pixels in the image that are classified correctly. It is the intersection of the predicted and true sets of pixels for a given class, divided by their union. A segmented ulcer that intersects with at least 50% of its ground truth is considered as true positive otherwise it is considered as false positive. A ground truth ulcer that has no corresponding segmented object or has less than 50% of its area overlapped by its corresponding segmented object is considered as a false negative. To evaluate the pixel accuracy in the proposed method the sensitivity and specificity measures are also considered. Sensitivity (also called the true positive rate, the recall, or probability of detection in some fields) measures the proportion of actual positives that are correctly identified. On the other hand, specificity (also called the true negative rate) measures the proportion of actual negatives that are correctly identified.

The sensitivity and specificity are then illustrated as:

$$Sensitivity = \frac{TP}{TP + FN} \tag{4.4}$$

$$Specificity = \frac{TN}{FP + TN} \tag{4.5}$$

Where;

TP is the number of true positives, FP is the number of false positives, and FN be the number of false negatives.

(ii) Dice Similarity

The Dice similarity coefficient is used as a statistical validation metric to evaluate the performance of both the reproducibility of manual segmentations and the spatial overlap accuracy of automated probabilistic fractional segmentation of the images (Zou *et al.*, 2004).

$$Dice = \frac{2 * TP}{(2 * TP + FP + FN)} \tag{4.6}$$

(iii) Matthew Correlation Coefficient (MCC)

To correctly evaluate the ulcer boundary determination the Matthew Correlation Coefficient is employed. The MCC returns a value between -1 (total disagreement) and +1 (perfect prediction) and is expressed as:

$$MCC = \frac{TP \times TN - FP \times FN}{\sqrt{(TP + FP)(TP + FN)(TN + FP)(TN + FP)}} \tag{4.7}$$

(iv) Jaccard Similarity Coefficient

This similarity measure is defined as the size of the intersection of the sets divided by the size of their union (Candemir *et al.*, 2014). The Jaccard Similarity Coefficient is the agreement between ground-truth image GT and the estimated segmentation mask S over all pixels in the image is given by:

$$\Omega = \frac{S \cap GT}{S \cup GT} = \frac{TP}{FP + TP + FN} \tag{4.8}$$

To execute this in MATLAB, the command *similarity = jaccard (S,GT)* is used to compute the intersection of the binary images of the output segmentation result and the ground truth divided by their intersection, also known as the Jaccard index.

CHAPTER FOUR

RESULTS AND DISCUSSION

4.1 Edge Detection Evaluation Results

From the conducted experiments, the visual results demonstrate that the proposed method outperforms in several cases when compared with some state-of-the-art classical methods. These experiments show that the new approach generates appealing images that are more detailed in a way that clearly defines the foot ulcer area which is the region of interest as illustrated in Fig. 12. The proposed method also produced appealing images as shown in Fig. 13 after adding noise to the images under test to simulate real-world situations where an image could also be noisy due to random disturbances.

Objective evaluation results further demonstrate higher values of PSNR and MSSIM depicted by the proposed method compared with the classical methods (Table 2 and Table 3). This objective evaluation confirms the effectiveness of the strategy used to formulate the edge detector. Combining diffusivities of the Total variation and the Perona-Malik mask their weaknesses, and hence the combination may generate more plausible edges. However, the tuning constants must be carefully selected to ensure better results. On the other hand, the canny operator shows the least average PSNR. These visual results suggest that this operator detects weak edges, a consequence that signals a possible generation of the unrequired false edges.

Furthermore, the proposed method is computationally efficient as shown in Table 4. Therefore, the method can be implemented into the actual hardware to segment foot ulcer images in practical settings. Given the promising results, an extension of this approach to such hardware may provide a revealing experience to the healthcare industry.

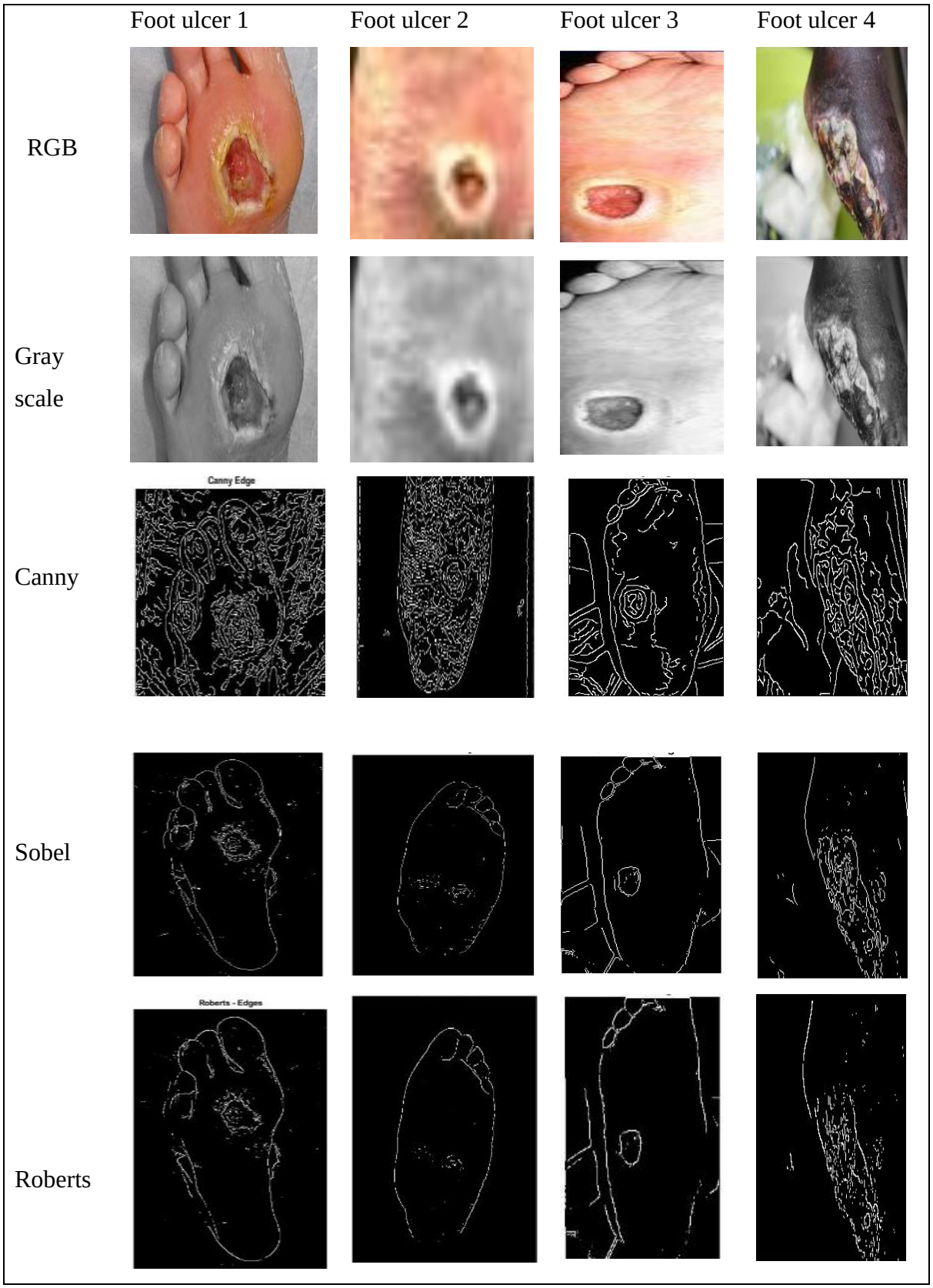

Figure 12: Edge Maps Generated by Sobel, Canny and Roberts Edge Detectors

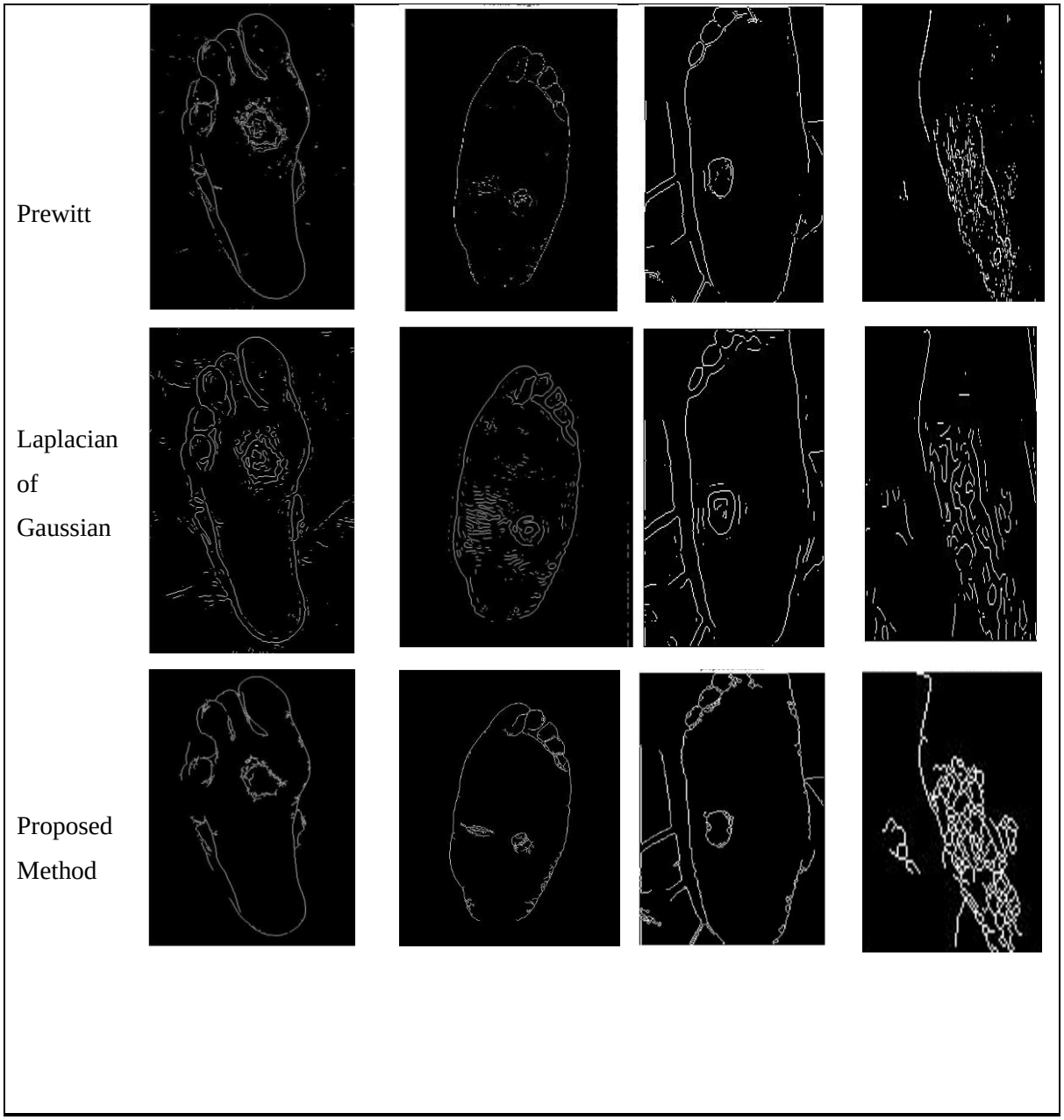

Figure 13: Edge Maps Generated by Prewit, Laplacian and the Proposed Method

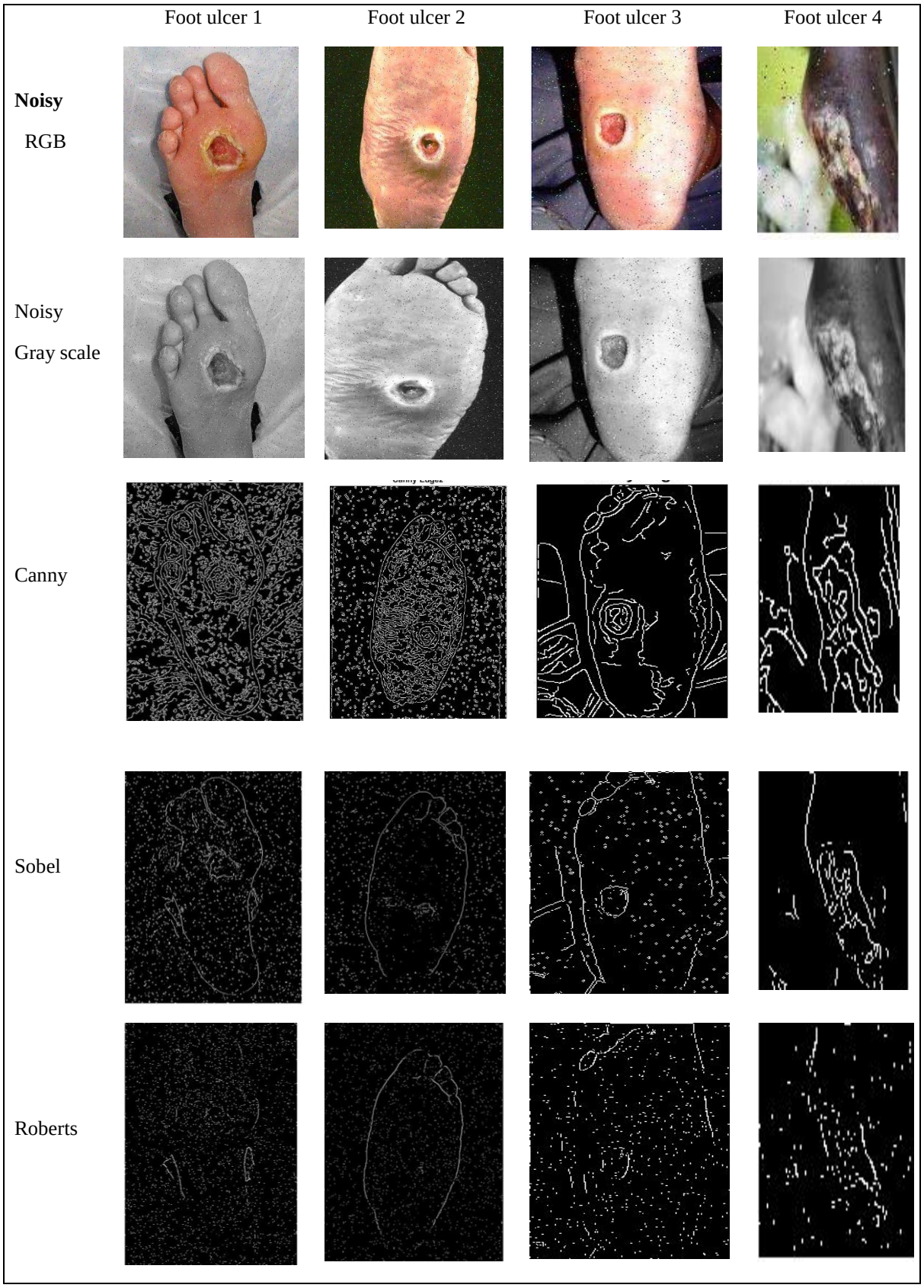

Figure 14: Simulated Results of Different Methods for Noisy Images

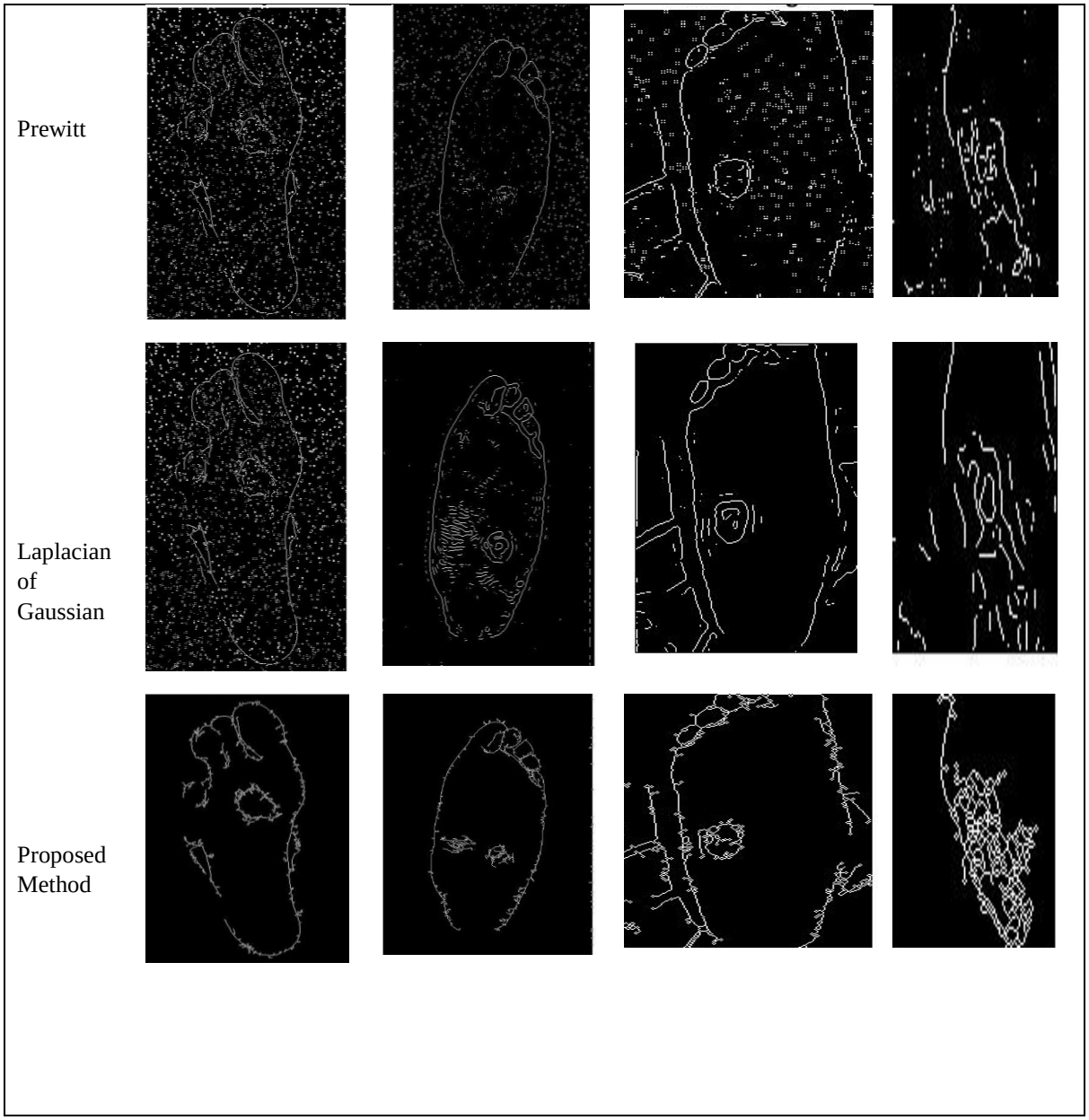

Figure 15: Results of Edge Detectors and the Proposed Method for Noisy Images

Table 2: Peak-Signal-To-Noise-Ratio Generated by Different Edge Detectors Applied on the Foot Ulcer Images (Input Images Contain Salt And Pepper Noise)

Images	Canny	Sobel	Roberts	Prewitt	LoG	Proposed Method
Foot Ulcer 1	53.84	59.36	61.04	59.30	60.44	63.28
Foot Ulcer 2	56.98	60.33	60.61	60.42	63.95	63.84
Foot Ulcer 3	55.34	59.01	61.19	59.19	62.76	65.98
Foot Ulcer 4	56.17	58.77	59.91	58.76	63.02	63.13
Foot Ulcer 5	54.25	59.54	62.30	59.10	60.00	66.97
Average	55.32	59.40	61.01	59.35	62.04	64.64

Table 3: MSSIM Values Generated by Edge Detectors Under Test

Images	Canny	Sobel	Roberts	Prewitt	LoG	Proposed Method
Foot Ulcer 1	0.9899	0.9974	0.9983	0.9974	0.9983	0.9985
Foot Ulcer 2	0.9941	0.9979	0.9981	0.9981	0.9994	0.9989
Foot Ulcer 3	0.9953	0.9984	0.9993	0.9986	0.9996	0.9996
Foot Ulcer 4	0.9934	0.9971	0.9979	0.9971	0.9992	0.9995
Foot Ulcer 5	0.9904	0.9974	0.9989	0.9970	0.9981	0.9993
Average	0.9926	0.9976	0.9985	0.9977	0.9989	0.9992

Table 4: Execution Time (in Seconds) of the Edge Detectors Under Test

Images	Canny	Sobel	Roberts	Prewitt	LoG	Proposed Method
Foot Ulcer 1	0.249	0.176	0.167	0.155	0.194	0.176
Foot Ulcer 2	0.288	0.178	0.155	0.188	0.177	0.163
Foot Ulcer 3	0.184	0.161	0.157	0.157	0.160	0.157
Foot Ulcer 4	0.187	0.176	0.281	0.243	0.331	0.178
Foot Ulcer 5	0.178	0.150	0.158	0.150	0.146	0.144
Average	0.217	0.168	0.184	0.179	0.202	0.163

4.2 Segmentation Validation Results

4.2.1 Segmentation Without an Edge Stopping Function

To visually evaluate the accuracy of the proposed method, the visual results from the well-known Chan-Vese segmentation algorithm (Chan & Vese, 2001) is compared to the proposed method. The Chan-Vese technique deforms an initial curve drawn on the ulcer image so that it separates foreground from background based on the means of the two regions. From the conducted experiments, it can be observed that the method gives better results when there is a clear difference between the foreground and background means as illustrated in Fig. 14. Furthermore, this technique is very robust to initialization in a way that the initial curve can be anywhere in the ulcer image, and interior contours of the ROI are automatically detected.

Despite its benefits, this method still has some drawbacks. Foremost, as this technique is based on intensity average only hence it tends to under-perform when tested for most of the ulcer images. The performance in terms of pixel accuracy, similarity measures and boundary determinations is shown in Table 5.

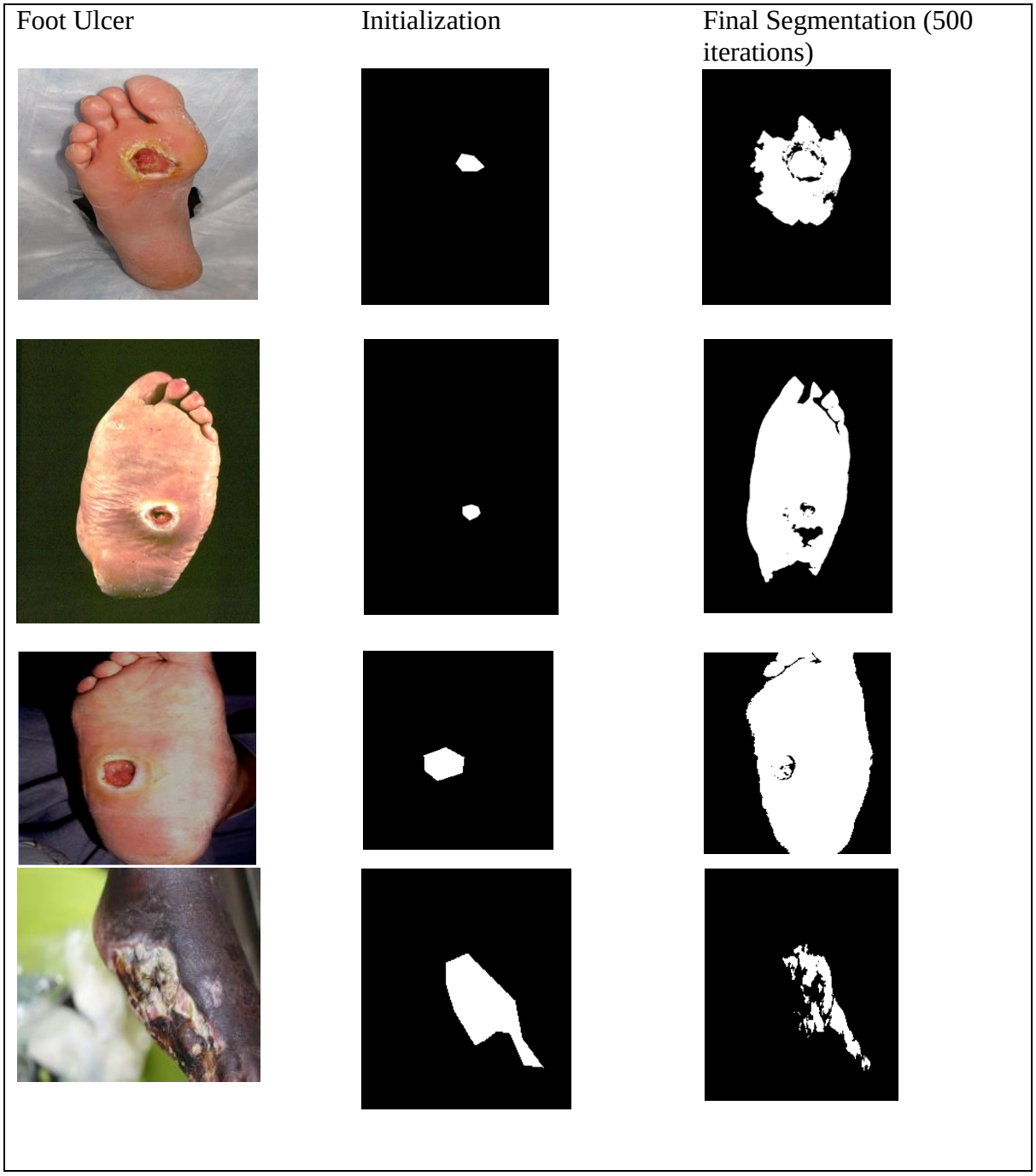

Figure 16: Active Contours Without Edges

Table 5: Validation Metrics Using the Chan-Vese Segmentation Method

Images	Accuracy	Sensitivity	Specificity	Precision	MCC	DICE	JACCARD
Foot ulcer 1	0.8400	0.9224	0.8385	0.0944	0.2656	0.1712	0.0936
Foot ulcer 2	0.7149	0.7258	0.7148	0.0137	0.0715	0.0269	0.0136
Foot ulcer 3	0.4854	0.8282	0.4795	0.0269	0.0798	0.0521	0.0268
Foot ulcer 4	0.6180	0.5443	0.6416	0.3272	0.1624	0.4087	0.2569

4.2.2 Localized Region Segmentation Results

To further find the best ulcer segmentation method, the results of a hybrid method based on analysis of the image statistics in small local regions as a means to separate the foreground from the background is then compared to the proposed method. This technique combines two methods of gradient-based active contours and region-based active contours with the aim of blending the benefits of the geodesic active contours and the region based active contours (Lankton & Tannenbaum, 2008). Figure 17 illustrates how this method is more versatile than the Chan-Vese active contours without edges. As with all geometric active contours methods this method is also subject to initial curve placement. Although it has reduced dependency on the initial curve the results from this method can not accurately locate the ulcer area in the image.

A major disadvantage of the method is illustrated in Fig. 16. This method fails to have an output when small sized images are tested due to the use of a global threshold value. From the experiments the images that have both their width and height below 300 pixels have no output regardless where the initial curve is placed.

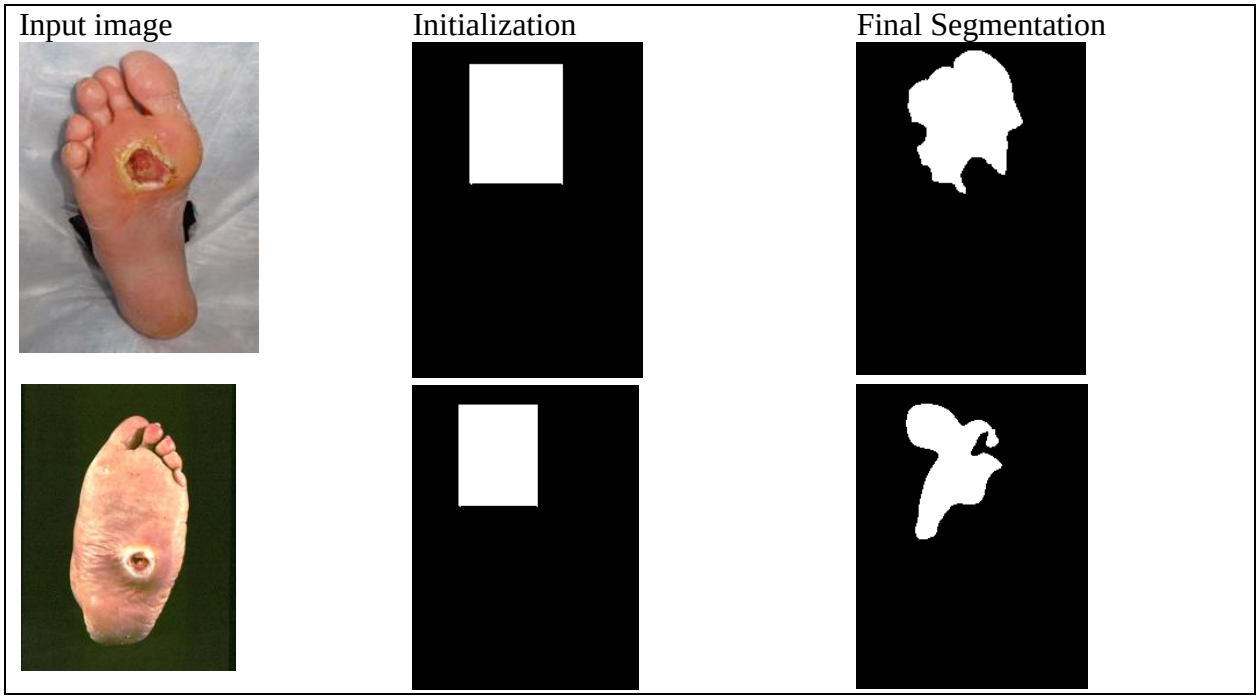

Figure 17: Localized Active Contours

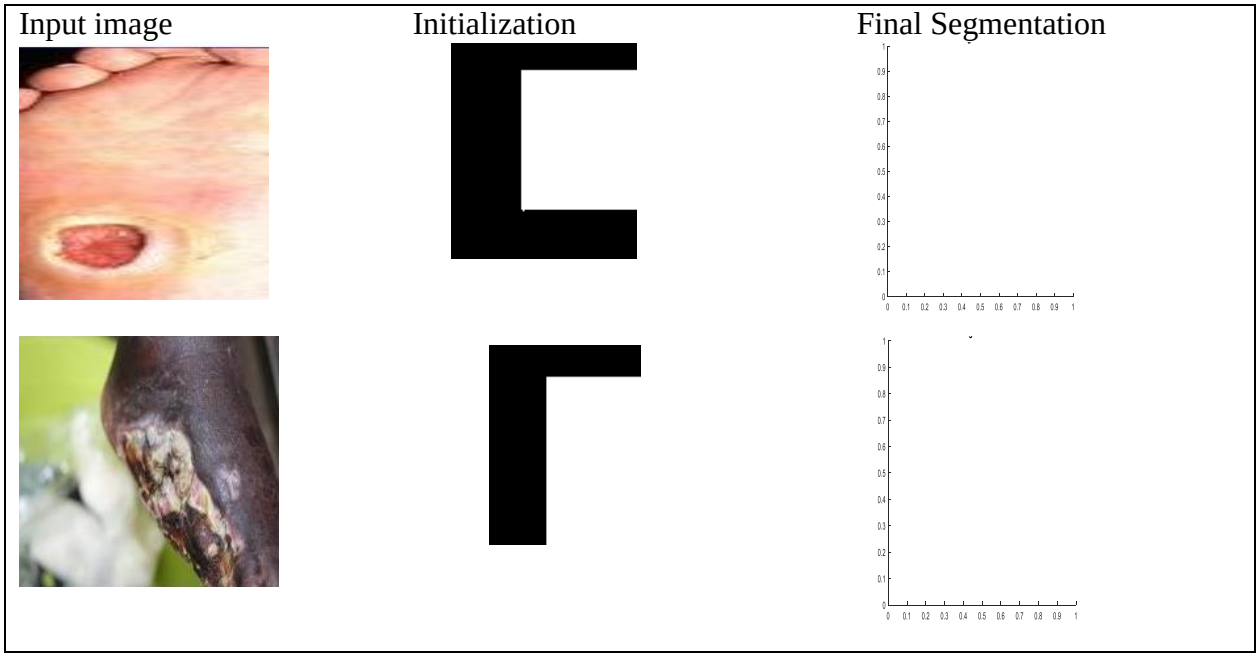

Figure 18: Localized Active Contours for Smaller Sized Images

4.2.3 The Proposed Segmentation Method Results

The results of the proposed method are then illustrated in Fig. 17. Compared to the active contours without edges and the localized method, the proposed method achieves better output segmentation results.

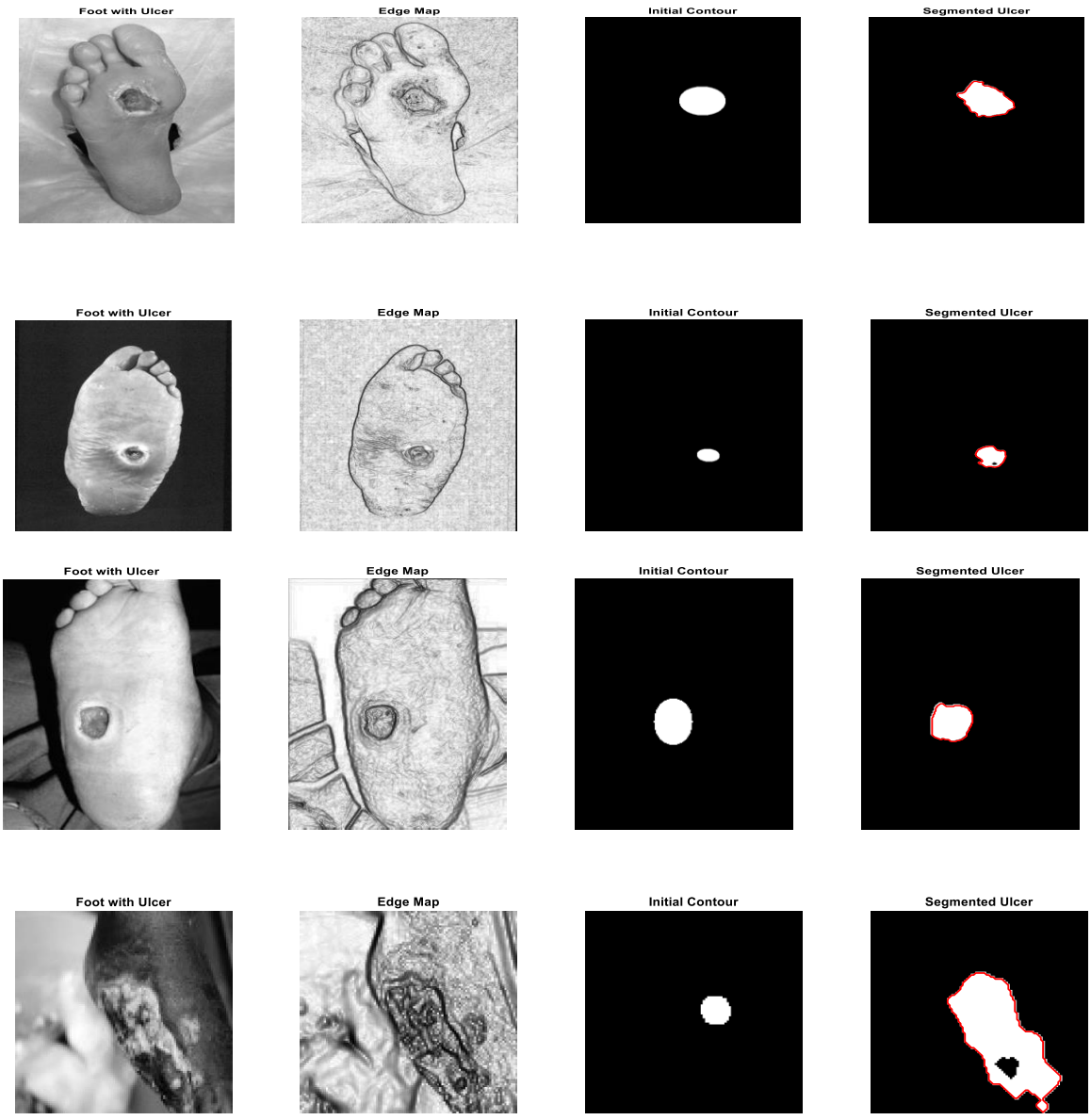

Figure 19: Proposed Segmentation Method

The visual results for comparison between the original ground truth image and resulting segmentation mask with the TP, TN and FP is shown in Fig. 18. The TP (white color) represents correctly classified ulcer pixels, FP (magenta color) represents pixels that are classified as

ulcers but are in fact background and FN (lime color) represents pixels that are classified as background but that are in fact part of the ulcer .

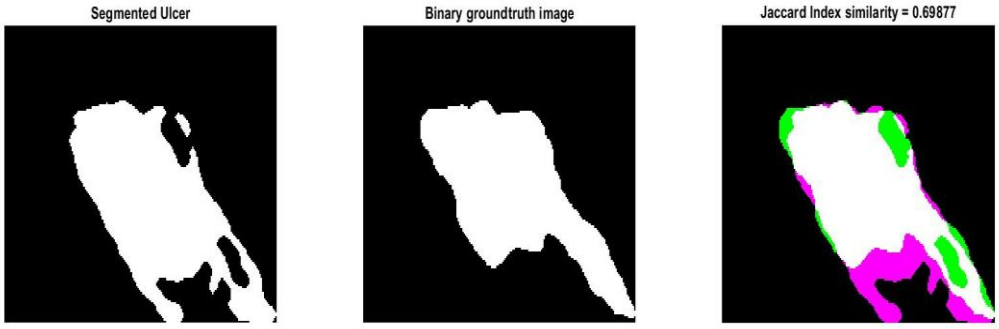

Figure 20: Visual Results for Similarity Measures

The results are then illustrated in Table 6 below in which the proposed method achieves promising results. The average scores for pixel accuracy, Jaccard, Dice score and MCC of the method are shown. From these results it can be observed that the segmentation method achieves higher pixel accuracy as well as higher similarity scores after incorporating the edge detection method as a pre-processing step before the overall segmentation. The comparison of the average validation metrics between the proposed method and the Chan-Vese without edges is shown in Table 7. The results proves that the proposed method is superior achieving values above 50% for each metric.

Table 6: Validation metrics for the Proposed Segmentation Method

Images	Accuracy	Sensitivity	Specificity	Precision	MCC	DICE	JACCARD
Foot ulcer 1	0.9942	0.9943	0.9942	0.7729	0.874	0.8697	0.7694
Foot ulcer 2	0.9981	0.6952	0.9995	0.8599	0.7723	0.7689	0.6245
Foot ulcer 3	0.9968	0.9385	0.9979	0.887	0.9108	0.912	0.8383
Foot ulcer 4	0.966	0.8947	0.9788	0.8843	0.8694	0.8895	0.8009

Table 7: Comparison of the Validation Metrics of the Method Under Test

Method	Accuracy	Sensitivity	Specificity	Precision	MCC	DICE	JACCARD
Chan-Vese method (Without edges)	0.6646	0.7552	0.6686	0.1156	0.1448	0.1647	0.0977
Proposed method (Incorporates edges)	0.9888	0.8807	0.9926	0.8510	0.8566	0.8600	0.7583

4.3 Discussion of the Results

Overall experimental results demonstrate the superiority of the proposed approach in terms of removing the false edges and improving the visual appeal of the segmentation output. The superior results of objective performance measures such as the peak signal-to-noise ratio PSNR, Mean Structural Similarity (MSSIM) and dice similarity values demonstrate the accuracy of the proposed method. The improvement of the results is due to the combination of the edge-preserving models of Perona Malik and Total Variation and thereafter employing active contours to segment the ulcers from the resulting output edge map.

The proposed method has also achieved the objective of being fast computationally. This has been demonstrated by having the least average execution time when compared to the existing classical methods. Such results prove that the proposed method is feasible to be implemented in actual hardware for time sensitive evaluation tasks.

CHAPTER FIVE

CONCLUSION AND RECOMMENDATIONS

5.1 Conclusion

In this work, the segmentation method for diabetic foot ulcers from digitally photographed images is proposed. This method combines the edge-preserving models of Perona Malik and Total Variation and thereafter employs active contours to segment the ulcers from the resulting output edge map. In this study, a novel image edge detection technique based on the combination of total variation (TV) and anisotropic diffusion (PM) models is presented. The technique used is by energy minimization and partial differential equations. The benefits of the new method on various images to locate the ulcer edges and ultimately segment them from the rest of the background is thus illustrated.

More specifically, the TV filter is applied to the areas which suffer from double and false edges, whereas, the anisotropic diffusion filter is applied to the areas which suffer from weak and discontinuous edges. Applying TV filter on the double edges areas will allow one to remove most of the false edges, and thus to obtain much sharper edges. While applying the anisotropic diffusion filter on the discontinuous edges areas will lead to obtaining robust and continuous edges. Consequently, less false edges besides high localization accuracy were obtained.

After getting the edge map active contours that deform to delineate the ulcer area are used. These deformable models are capable of accommodating the significant variability of the ulcer structures over time and across different individuals. Furthermore, they support highly intuitive interaction mechanisms that, when necessary, will allow DFU specialists and practitioners to bring their expertise to bear on the model-based image interpretation task.

Experimental results further demonstrate the superiority of the proposed approach in terms of removing the false edges and improving the appeal of the segmentation output. As objective quantitative performance measures, the peak signal-to-noise ratio (PSNR), Mean Structural Similarity (MSSIM) and the average execution time were used for evaluation and comparison to the existing methods.

This research has thus laid the foundation that could be used to provide both practical and theoretical understanding for future works in the segmentation of diabetic foot ulcers from digital images. The contribution has been made through:

(i) Establishment of an edge detector that combines both the features of Perona-Malik and Total variation. The proposed method is computationally efficient, and, therefore, it can be implemented into actual hardware to segment foot ulcer images in practical settings.
(ii) Increasing the segmentation accuracy in terms of PSNR, MCC, and MSSIM by employing deformable models on the resulting edge map.

5.2 Recommendations

This research work can be expanded into a number of directions in the future. Foremost, this research recommends a further stabilization of the robustness of the proposed segmentation method, by expanding the diversity of the diabetic foot ulcer image database in terms of ulcer infection type, shape, the color composition for different skin types as well as surrounding tissues. Secondly, although the validation assessment results of the method show good agreement with clinicians' scores, more validation data is needed to further evaluate our method. Finally, the use of neural networks to extract more features and increase the accuracy of the segmentation method is also recommended.

REFERENCES

Acton, S. T., & Ray, N. (2009). Biomedical image analysis segmentation. *International Journal of Multimedia and Image Processing*, 4(1), 1–18.

Al-rubeaan, K., Derwish, M., Ouizi, S., Youssef, A. M., Subhani, S. N., Ibrahim, H. M., & Alamri, B. N. (2015). Diabetic foot complications and their risk factors from a large retrospective cohort study. *Journal of PLoS ONE*, 10(5), 1-18.

Asmaidi, A., Putra, D. S., Risky, M., & Rahul, F. U. (2019). Implementation of sobel method based edge detection for flower image segmentation. *Journal of Sinkron*, 3(2), 161-169.

Assirati, L., Silva, N. R., Berton, L., Lopes, A., & Bruno, O. M. (2014). Performing edge detection by difference of gaussians using q-gaussian kernels. *Journal of Physics*, 49(1), 1- 6.

Bayraktar, M., Kockara, S., Halic, T., Mete, M., Wong, H. K., & Iqbal, K. (2019). Local edge-enhanced active contour for accurate skin lesion border detection. *Journal of Bioinformatics*, 20(2), 91-101.

Bennett, J. E., Stevens, G. A., Mathers, C. D., Bonita, R., Rehm, J., Kruk, M. E., …, Ezzati, M. (2018). Non Communicable Disease Countdown 2030: Worldwide trends in non-communicable disease mortality and progress towards sustainable development goal target. *Journal of the Lancet*, 392(10152), 1072–1088.

Berbar, M. A., Kelash, H. M., & Kandeel, A. (2006). Faces and facial features detection in color images. *Journal of Geometric Modeling and Imaging New Trends*, 206(1), 209–214.

Boulton, A. J., Vileikyte, L., Ragnarson,T. G., & Apelqvist, J. (2005). The global burden of diabetic foot disease. *Journal of the Lancet*, 366(9498), 1719–1724.

Candemir, S., Jaeger, S., Palaniappan, K., Musco, J. P., Singh, R. K., Xue, Z., …, McDonald, C. J. (2014). Lung segmentation in chest radiographs using anatomical atlases with nonrigid registration. *IEEE Transactions on Medical Imaging*, 33(2), 577–590.

Chalya, P. L., Mabula, J. B., Dass, R. M., Kabangila, R., Jaka, H., McHembe, M. D., …, Gilyoma, J. M. (2011). Surgical management of diabetic foot ulcers. *Journal of Bio-Medicine Research*, 4(1), 35-39.

Chan, T. F., & Vese, L. A. (2001). Active contours without edges. *IEEE Transactions on Image Processing*, 10(2), 266-277.

Chandwadkar, R., Dhole, S., Gadewar, V., Raut, D., & Tiwaskar, S. (2013). Comparison of edge detection techniques. *The 6th Annual Conference of Institute of Research and Journal* 6(2), 133-136.

Chiwanga, F. S., & Njelekela, M. A. (2015). Diabetic foot prevalence knowledge and foot self-care practices among diabetic patients in Tanzania. *Journal of Foot and Ankle Research*, 8(3), 20-28.

Cho, N. H., Shaw, J. E., Karuranga, S., Huang, Y., Rocha F. J. D., Ohlrogge, A. W., & Malanda, B. (2018). Global estimates of diabetes prevalence for 2017 and projections for 2045. *Journal of Diabetes Research and Clinical Practice*, 138(2), 271-281.

Davis, F. M., Kimball, A., Boniakowski, A., & Gallagher, K. (2018). Dysfunctional wound healing in diabetic foot ulcers. *Journal of Diabetes Research and Clinical Practice*, 11(8), 92-99.

Feng, Y., Zhang, J., & Wang, S. (2017). A new edge detection algorithm based on canny idea. *AIP Conference Proceedings*, 18(10), 163-172

Ferhat, A., Mohamed, A., Oussama, K., Messaoudi, K., & Boudjelal, A. (2013). Implementation of sobel prewitt roberts edge detection. *The World Congress in Computer Science, Computer Engineering, and Applied Computing*, 6(1), 23-30.

Goyal, M., Reeves, N. D., Davison, A. K., Rajbhandari, S., Spragg, J., & Yap, M. H. (2017). Convolutional neural networks for diabetic foot ulcer classification. *IEEE Journal of Biomedical and Health Informatics*, 20(3), 130–141.

Goyal, M., Reeves, N. D., Rajbhandari, S., & Yap, M. H. (2019). Robust methods for real-time diabetic foot ulcer detection and localization on mobile devices. *IEEE Journal of Biomedical and Health Informatics*, 23(4), 1730–1741.

Guidotti, P. (2012). A backward–forward regularization of the perona malik equation. *Journal of Differential Equations*, 252(4), 3226–3244.

Gupta, N., P Shukla, A., & Agarwal, S. (2016). Despeckling of medical ultrasound images. *International Journal of Information Engineering and Electronic Business*, 8(3), 11-19.

Kaur, D., & Kaur, Y. (2014). Various image segmentation technique. *International Journal of Computer Science and Mobile Computing*, 3(5), 809-814.

Kessy, S., Maiseli, B., & Kisangiri, M. (2017). Hybrid diffusion steered model for suppressing multiplicative noise in ultrasonograms. *International Journal of Signal and Image Processing*, 8(4), 01-13.

Kobayashi, H., Ogawa, M., Alford, R., Choyke, P. L., & Urano, Y. (2010). New strategies for fluorescent probe design in medical diagnostic imaging. *Journal of Chemical Reviews*, 110(5), 2620-2640.

Kumar J., & Malathy, A. (2016). Image processing based wound assessment system for patients with diabetes using six classification algorithms. *The International Conference on Electrical, Electronics, and Optimization Techniques*, 3(2), 744-747.

Lankton, S., Nain, D., Yezzi, A., & Tannenbaum, A. (2007). Hybrid geodesic region-based curve evolutions for image segmentation. *Journal of Medical Imaging*, 65(10), 65-71.

Lankton, S., & Tannenbaum, A. (2008). Localizing region-based active contours. *IEEE Transactions on Image Processing*, 17(11), 2029–2039.

Luo, S., Yang, J., Gao, Q., Zhou, S., & Zhan, C. A. (2017). The edge detectors suitable for retinal oct image segmentation. *Journal of Healthcare Engineering*, 7(3), 15-25.

Maini, R. (2009). Study and comparison of various image edge detection techniques. *International Journal of Image Processing*, 12(3), 35-42.

Maiseli, B. J., Elisha, O. A., & Gao, H. (2015). A multi-frame super-resolution method based on the variable-exponent nonlinear diffusion regularizer. *EURASIP Journal on Image and Video Processing*, 2015(1), 22-29.

Marr, D., & Hildreth, E. (1980). Theory of edge detection. *Journal of Biological Sciences*, 207(11), 187–217.

Mavrogenis, A. F., Megaloikonomos, P. D., Antoniadou, T., Igoumenou, V. G., Panagopoulos, G. N., Dimopoulos, L., ..., Lazaris, A. (2018). Current concepts for the evaluation and management of diabetic foot ulcers. *Journal of Efort Open Reviews*, 3(9), 513–525.

Morfu, S. (2010). Image processing using diffusion processes. *IEEE International Symposium on Circuits and Systems*, 7(2), 1811–1814.

Muthukrishnan, R., & Radha, M. (2011). Edge detection techniques for image segmentation. *International Journal of Computer Science and Information Technology*, 3(6), 259-267.

Nagaraju, C. (2017). Canny scale edge detection. *International Journal of Engineering Trends and Technology*, 9(5), 3-7.

Netten, J. V., Clark, D., Lazzarini, P. A., Janda, M., & Reed, L. F. (2017). The validity and reliability of remote diabetic foot ulcer assessment using mobile phone images. *Journal of Scientific Reports*, 7(1), 95-103.

Nouvong, A., Hoogwerf, B., Mohler, E., Davis, B., Tajaddini, A., & Medenilla, E. (2009). Evaluation of diabetic foot ulcer healing with hyperspectral imaging of oxyhemoglobin and deoxyhemoglobin. *Journal of Bio-Medicine Research*, 7(2), 68-75.

Olveres, J., Carbajal, D. E., Escalante, R. B., Vallejo, E., & García, C. M. (2017). Deformable models for segmentation based on local analysis. *Journal of Mathematical Engineering*, 10(3), 11-25.

Palma, C. A., Cappabianco, F. A. M., Ide, J. S., & Miranda, P. A. V. (2014). Anisotropic diffusion filtering operation and limitations of magnetic resonance imaging evaluation. *IFAC Journal of Systems and Control*, 19(3), 3887–3892.

Patterson, C., Karuranga, S., Salpea, P., Saeedi, P., Dahlquist, G., Soltesz, G., & Ogle, G. D. (2019). Worldwide estimates of incidence, prevalence and mortality of type one diabetes in children and adolescents. *International Journal of Diabetes Research and Clinical Practice*, 10(7) 842- 851.

Peng, B., Zhang, L., & Zhang, D. (2010). Automatic image segmentation by dynamic region merging. *International Journal of Image Processing*, 14(5), 135-142.

Pham, D. L., Xu, C., & Prince, J. L. (2000). Current methods in medical image segmentation. *Journal of Biomedical Engineering*, 2(1), 315–337.

Pratondo, A., Ong, S. H., & Chui, C. K. (2014). Region growing for medical image segmentation using a modified multiple-seed approach on a multi-core central processing unit computer. *International Federation of Medical and Biological Engineering*, 43(6), 112–115.

Saeedi, P., Petersohn, I., Salpea, P., Malanda, B., Karuranga, S., Unwin, N., …, Leonor, S. (2019). Global and regional diabetes prevalence estimates for 2019 and projections for 2030 and 2045. *International Journal of Diabetes Research and Clinical Practice,* 7(3), 115-125.

Selesnick, I. (2012). Total variation denoising. *The Matrix Journal*, 2012(0), 1–13.

Shah, P., Mahajan, S., Nageswaran, S., Paul, S. K., & Ebenzer, M. (2019). Non-contact ulcer area calculation system for neuropathic foot ulcer. *Journal of Foot and Ankle Surgery*, 25(1), 47–50.

Shahnoor, M., & Khan, I. (2012). Implementation of edge shape detection techniques and their performance evaluation. *International Journal of Image Processing,* 33(9), 205-212.

Sharma, A., Punjab, J., Pankaj, S. I., Rashmi, I., & Hardeep, K. I. (2012). Edge detection of medical images using morpholgical algorithms. *International Journal for Science and Emerging Technologies with Latest Trends,* 4(1), 1-6.

Shrivakshan, G. T. (2012). A comparison of various edge detection techniques used in image processing. *International Journal of Computer Science*, 9(5), 269–276.

Subhro, S., & Ardhendu, M. (2015). Comparison of some classical edge detection techniques with their suitability analysis for medical images processing. *International Journal of Computer Sciences and Engineering*, 3(1), 81–87.

Tang, L., & Fang, Z. (2016). Edge and contrast preserving in total variation image denoising. *EURASIP Journal on Advances in Signal Processing*, 2016(1), 1–21.

Tian, X. (2012). A novel image edge detection algorithm based on prewitt operator and wavelet transform. *International Journal of Advancements in Computing Technology*, 4(9), 73-82.

Tyagi, V. (2018). Understanding digital image processing. *Journal of Digital Image Processing*, 12(1), 97-105.

Varshney, P. S., Rajpal, N., & Purwar, R. (2009). Comparative study of image segmentation techniques and object matching using segmentation. *International Conference on Methods and Models in Computer Science*, 2009(53), 79-85.

Vincent, O., & Folorunso, O. (2009). A descriptive algorithm for sobel image edge detection. *Proceedings of the 2009 Informing Science and Information Technology Education Conference*, 10(2), 33-51.

Wang, P. C., Agu, E., Strong, D., & Tulu, B. (2019). Boundary determination of foot ulcer images by applying the associative hierarchical random field framework. *Journal of Medical Imaging*, 6(2), 117-186.

Wang, P. C., Strong, D. M., Tulu, B., Agu, E., Ignotz, R., & Henry, Q. (2015). An automatic assessment system of diabetic foot ulcers based on wound area determination, color segmentation, and healing score evaluation. *Journal of Diabetes Science and Technology*, 10(2), 421-428.

Wang, P. C., Strong, D., Tulu, B., & Agu, E. (2013). Wound image analysis system for diabetics. *International Journal of Diabetes Research and Clinical Practice*, 5(9), 95-104.

Wang, Z., Bovik, A. C., Sheikh, H. R., & Simoncelli, E. P. (2004). Image quality assessment: from error visibility to structural similarity. *IEEE Transactions on Image Processing*, 13(4), 90-100.

Yan, J., & Shu, L. Z. (2013). Image denoising based on the modied rof model. *International Conference on Multimedia Technology*, 11(9), 1106–1114.

Yang, L., Wu, X., Zhao, D., Li, H., & Zhai, J. (2011). An improved prewitt algorithm for edge detection based on noised image. *Proceedings of the 4th International Congress on Image and Signal Processing*, 2011(3), 1197–1200.

Yap, M. H., Pons, G., Martí, J., Ganau, S., Sentís, M., Zwiggelaar, R., Davison, A. K., & Martí, R. (2018). Automated breast ultrasound lesions detection using convolutional neural networks. *IEEE Journal of Biomedical and Health Informatics*, 22(4), 1218–1226.

Zeng, G. L. (2015). On few-view tomography and staircase artifacts. *IEEE Transactions on Nuclear Science*, 62(3), 851–858.

Zhichang, G., Jiebao, S., Dazhi, Z., & Boying, W. (2012). Adaptive perona–malik model based on the variable exponent for image denoising. *IEEE Transactions on Image Processing*, 21(3), 958–967.

Zhou, W. & Bovik, A. C. (2009). A new look at signal fidelity measures. *IEEE Signal Processing*, 26(1), 98–117.

APPENDICES

Appendix 1: Research Ethical Clearance Certificate

Kibong'oto Infectious Diseases Hospital- Nelson Mandela African Institution of Science and Technology- Centre for Educational Development in Health, Arusha (KIDH-NM-AIST-CEDHA) -KNCHREC

RESEARCH ETHICAL CLEARANCE CERTIFICATE

Research Proposal No: KNCHREC0015 **3rd May 2019**

Study Title: Development of a Fast and Accurate Method for Segmentation of Diabetic Foot Ulcers Images

Study Area: THE NELSON MANDELA AFRICAN INSTITUTION OF SCIENCE AND TECHNOLOGY

PI Name: Rehema Hamis Mwawado
Co-Invigilator:
Institutions: **The school of Computational and Communication Science and Engineering (CoCSE)**

The Proposal has been approved by KNCHREC on 3rd May 2019

1. Subject to this approval you will be required to submit your progress report to the KNCHREC, National Institute of Research and Ministry of Health Community Development Gender Elderly and Children
2. Publication of your findings is subject to presentation to the KNCREC and NIMR Approval.
3. Copies of final publication should be made available to KNCHREC, National Institute of Research and Ministry of Health Community Development Gender Elderly and Children
4.

Duration of Study Renewal: Subject to Renewal within ONE YEAR
Span From: 3rd May 2019 to 2nd May 2020.

.....
Mr. Simon Njeya
Secretary
KNCHREC

Chairperson
KNCHREC

Appendix 2: Arusha Regional Office Research Permit

THE UNITED REPUBLIC OF TANZANIA
PRESIDENT'S OFFICE
REGIONAL ADMINISTRATION AND LOCAL GOVERNMENT

MKOA WA ARUSHA
Anwani ya simu "REGCOM"
Simu Na. 2545608/ 2545820/ 2545872
Fax Na. 2545239/ 2544386
E-Mail: rasarusha@yahoo.com
E-Mail: rasarusha@gmail.com

DISTRICT COMMISSIONER'S OFFICE
P.O.BOX 1,
ARUSHA

Unapojibu tafadhali taja:

Ref. Na. AB. 361/411/01/104 **11th March, 2019**

Medical Officer In charge,
Mount Meru Regional Hospital,
P.O. BOX.
ARUSHA.

RE: RESEARCH PERMIT

Reference is hereby made to the letter Ref. FA.195/223/01'L'/44 dated 8th February, 2019 from the Regional Commissioner's Office.

I hereby take this opportunity to introduce to you **Ms. Rehema Hamisi Mwawado** from The Nelson Mandela African Institution of Science and Technology (NM-AIST). At the moment conducting a research titled: ***"Development of a Fast and Accurate Methods for Segmentation of Diabetic Foot Ulcers Images".***

The above has been granted permission to conduct his research in our district of Arusha from **11 February, 2019.**

Due to this, you are requested to render any necessary Administrative Assistance to enable her to accomplish the intended objective of his research.

Thank you for your cooperation.

N.L. Wailiba,
For: DISTRICT ADIMINISTRATIVE SECRETARY
ARUSHA.

Copy to:
Ms. Rehema Hamisi Mwawado.

KAI BU TAWALA (W)
WILAYA YA ARUSHA

Appendix 3: Research Permit, Arusha Regional Hospital

THE UNITED REPUBLIC OF TANZANIA
MINISTRY OF HEALTH, COMMUNITY DEVELOPMENT, GENDER, ELDERLY AND CHILDREN

Telegrams: **"REGCOM"**
Telephone: 250-335751 -2
Fax: 2544904
Website: www.arusha.go.tz
E-mail: mt.merurrh@afya.go.tz
In reply please quote:

RMO/ARS/F-1/14C/103

REGIONAL REFERRAL HOSPITAL,
P.O. Box 3092,

ARUSHA

10th May, 2019.

Ms.Rehema Hamis Mwawando,

Nelson Mandela Institution of Science and Technology,

P.o.Box 447,

Arusha.

Re: Research Permit

Refer to the subject matter above, as well as your research permit with reference No.AB.361/411/01/104 dated 11th March 2019.

Our office is permitting you a period of two weeks to stay in this Hospital commencing 13th May up to 25th May 2019 purposely for collecting data concerning your research study .If you will need more time, you will request for extension of permit.

Counting your good cooperation .

(Gerald Philip)

For: MEDICAL OFFICER IN CHARGE

ARUSHA

Copy to: Surgical Ward.

Appendix 4: Informed Consent Sample Form, English Version

THE NELSON MANDELA

AFRICAN INSTITUTION OF SCIENCE AND TECHNOLOGY

(NM-AIST)

School of Computational and
Communication Sciences and Engineering

Direct Line: +255 272970001
Fax: +255272970016
E-mail: dean-cocse@nm-aist.ac.tz

Tengeru
P.O. Box 447
Arusha, TANZANIA
Website: www.nm-aist.ac.tz

ID-No: M441/T.17

Introduction

Greetings! My name is Rehema Hamis Mwawado, a Master student specializing in Electronics and Communication Sciences at The Nelson Mandela African Institution of Science and Technology. I am conducting a research on; Development of a Fast and Accurate Method for Segmentation of Diabetic Foot Ulcers Images.

Purpose of the study

For individuals with Diabetes Mellitus, foot ulcers represent a significant health issue. Across the globe, 40-60% of all lower extremity non-traumatic amputations are performed in patients with diabetes. Current clinical approaches to DFU treatment rely on the vigilance of both the patient and clinician. Less accurate assessment methods, time-consuming diagnostic procedures and relatively high treatment costs are among the limitations of the existing practices. Technology employing image analysis techniques is a potential solution to address issues of the inaccuracy of the visual assessment as well as minimizing consecutive patient visits to the clinics. This work proposes a diabetic foot ulcer image segmentation method that avoids complex geometric and mathematical modelling and guarantees high accuracy in ulcer segmentation and therefore low segmentation error rate of the foot ulcer images. This work aims to become a paving step in developing a complete mobile imaging system that can be validated clinically in the future and help diabetic patients in Tanzania and the world at large.

What Participation Involves

If you agree to participate in this study the following will occur:

A high resolution camera and a low resolution camera will be used to capture the images of the foot ulcers. Whenever possible, the images will be acquired with close-ups of the full foot with the distance of around 30-40 cm with the parallel orientation to the plane of Diabetic foot ulcer.

Confidentiality

I assure you that all the information collected from you will be kept confidential. Only people working in this research study will have access to the information. We will not put your name or other identifying information on the records of the information you provide.

Risks

A patient might be uncomfortable due to position the foot when getting the right angle for capturing the foot ulcer image.

Rights to Withdraw and Alternatives

Taking part in this study is completely your choice. If you choose to participate in the study or if you decide to stop participating in the study you will not get any harm. Refusal to participate or withdrawal from the study will not affect the quality of health care service that you receive from the health care facility.

Benefits

There will be no direct benefit to you; however the information you provide and the images captured will be a paving step in developing a complete affordable mobile imaging system that can be validated clinically in the future and help diabetic patients in Tanzania and the world at large.

In Case of Injury

We do not anticipate that any harm will occur to you as a result of participation in this study.

Who to contact

If you have questions about this study and more clarifications regarding right as a participant or any other study related questions, Please contact me as the Principal **Investigator.** My address is Rehema Mwawado, The Nelson Mandela African Institution of Science and Technology, P.O. Box 447, Arusha, Tanzania (Mobile. no. 0656830449 or 0767509905).

Certification of consent

I have been invited to take part in the study on Development of a Fast and Accurate Method for Segmentation of Diabetic Foot Ulcers Images. I have read the foregoing information or it has been read to me and has understood. My questions have been answered to my satisfaction. I agree to participate in this study.

Signature

Do you agree?

Participant Agrees [ ] Participant disagree [ ]

Signature (or thumbprint) of participant: ……. Date: …….

Signature of witness (if the participant cannot read): ……. Date: …….

Signature of the principal investigator: ……. Date: …….

Appendix 5: Fomu ya Ridhaa ya Kushiriki Kwenye Utafiti, (Swahili Version)

THE NELSON MANDELA

AFRICAN INSTITUTION OF SCIENCE AND TECHNOLOGY

(NM-AIST)

School of Computational and
Communication Sciences and Engineering

Tengeru

Direct Line: +255 272970001

Fax: +255272970016

E-mail: dean-cocse@nm-aist.ac.tz

P.O. Box 447

Arusha, TANZANIA

Website: www.nm-aist.ac.tz

Namba ya utambulisho: ……

Utambulisho

Salaam! Mimi naitwa Rehema Mwawado, mwanafunzi wa shahada ya pili katika Taasisi ya kiafrika ya sayansi na teknologia Nelson Mandela. Ninafanya utafiti wa wa kutengeneza mfumo wakutumia njia za kikompyuta zilizo haraka na sahihi zaidi ambazo hutumia picha iliyopigwa na kamera kutambua vidonda vya kwenye miguu kwa wagonjwa wa kisukari

Lengo la utafiti

Kazi hii inalenga kuwa hatua ya kutengenezea na kuendeleza mfumo kamili wa picha ya simu ambayo ni nafuu zaidi na inaweza kuthibitishwa kikliniki baadaye na kusaidia wagonjwa wa kisukari nchini Tanzania na duniani kwa ujumla.

Nini kinahusika unaposhiriki

Kama unakubali kushiriki katika utafiti huu yafuatayo yatafanyika:

Kamera itatumika kupata picha za vidonda vya miguu. Kila iwezekanavyo, picha zitapatikana kwa karibu ya mguu kamili na umbali wa karibu 30-40 cm kutoka kwenye kidonda cha mguu.

Usiri

Ninakuhakikishia kwamba taarifa zote zitakazopatikana kutoka kwako zitakuwa siri. Ni watafiti pekee wanaofanya kazi katika utafiti huu ndio watakaoweza kuzifahamu taarifa hizo.

Hatutaweka jina lako au taarifa yoyote inayokutambulisha wewe katika rekodi ya taarifa ulizotoa.

Hatari

Mgonjwa ataweza kupata usumbufu kidogo kutokana na jinsi mguu utavyowekwa katika upigaji wa picha.

Haki ya kujitoa au vinginevyo

Ni uamuzi wako kushiriki katika utafiti huu. Unaweza kusitisha ushiriki wako katika utafiti huu muda wowote hata kama ulishatoa ridhaa ya kushiriki. Kukataa kushiriki au kujitoa katika utafiti hakutaathiri ubora wa huduma ya afya unayopata kutoka katika kituo cha afya husika.

Faida

Hapatakuwa na faida moja kwa moja kwako; hata hivyo picha zilizo pigwa zitasaidia kuwa hatua ya kupanua na kuendeleza mfumo kamili wa picha za simu za bei nafuu ambazo zinaweza kuthibitishwa kikliniki baadaye na kusaidia wagonjwa wa kisukari nchini Tanzania na duniani kwa ujumla

Endapo utapata madhara au la

Hatutarajii kuwa madhara yoyote yatatokea kwako kama matokeo ya kushiriki katika utafiti huu.

Nani wa kuwasiliana nae

Kama utakuwa na maswali juu ya utafiti huu na haki ya mtoto wako kama mshiriki au maswali yoyote yanayoendana na utafiti huu, tafadhari wasiliana na mimi kama mtafiti mkuu**.** Anuani yangu ni Rehema Mwawado, Taasisi ya kiafrika ya sayansi na teknologia Nelson Mandela, S.L.P 447, Arusha, Tanzania (simu 0656830449 or 0767509905).

Kuthibitisha ridhaa

Nimekaribishwa kushiriki katika utafiti wa kutengeza mfumo wakutumia njia za kikompyuta zilizo haraka na sahihi zaidi ambazo hutumia picha iliyopigwa na kamera kutambua vidonda vya kwenye miguu kwa wagonjwa wa kisukari. Nimesoma taarifa au imesomwa kwangu na kuielewa. Maswali yangu yamejibiwa na nimeridhika hivyo ninakubali kushiriki katika utafiti huu.

Saini

Unakubali?

Mshiriki anakubali [✓]

Mshiriki anakataa [__]

Saini(au alama ya kidole gumba) ya mshiriki:..... Tarehe: 14/05/2019

Saini ya shahidi(kama mshiriki hawezi kusoma): ..... Tarehe: .....

Saini ya mtafiti mkuu:..... Tarehe: 14/05/2019

Appendix 6: The Proposed Segmentation Method MATLAB Code[1]

```
%Read the input image
I = imread('footulcer1.jpg');

%Perform  the ulcer Segmentation
u=dfu_proposed_method(I);

%----------------------------AUXILIARY FUNCTIONS----------------------------------------

function edges_u =dfu_proposed_method(u)
%Convert the input image to a double grayscale
if size(u,3)==3
   u=rgb2gray(u);
end
k1=20;
k2=100;
u = double(u);

%find the image  gradient
[ux, uy] = gradient(u);
grad_u = sqrt(ux.^2 + uy.^2);

%proposed edge detector
edges_u = 1./(1 + (grad_u/k1) + (grad_u/k2).^2);

% Display the edge map
I2 = edges_u;
imshow(I2)

% Draw an ellipse around the ROI
R=get_ellipse(I2);
imshow(R)

% Use active contours to segment the ulcer area and display the results
m = zeros(size(I2));
m(R) = true;
seg = dfu_seg2(edges_u,m,500);

seg= medfilt2(seg (:,:,1), [7 7]);
k0= strel('disk', 2);
Io = imopen(seg , k0);
Ic = imclose(Io, k0);

ulcer=Ic;
figure(6);
```

[1] https://in.mathworks.com/matlabcentral/fileexchange/73965-edge-detection-method-for-dfu-images

```
subplot(1,4,1);

imshow(u,[]);
title('Foot with Ulcer');

subplot(1,4,2);
imshow(I2,[]);
title('Edge Map');

subplot(1,4,3);
imshow(R);
title('Initial Contour');

subplot(1,4,4);
imshow(ulcer,[]);
title('Ulcer Alone');

[B,l]=bwboundaries(ulcer,'noholes');
subplot(1,4,4);

imshow(ulcer,[]);
hold on
for i=1:length(B)
   plot(B{i}(:,2),B{i}(:,1), 'r' ,'linewidth',1.45);


end

title('Segmented Ulcer');
hold off;

end

%----------------------------ACTIVE CONTOURS---------------------------------------

%Inputs: I           2D image
%       init_mask   Initialization of the mask (1 = foreground, 0 = background)
%       max_ite     Number of iterations to run segmentation
%       alpha       (optional) Weight of smoothing term
%                   default = 0.2
%       display     displays intermediate outputs
%                   default = true


% Outputs: seg        Final segmentation mask (1=foreground, 0=background)

function seg = dfu_seg2(I,init_mask,max_ite,alpha,display)
%-- default value for parameter alpha is .2
 if(~exist('alpha','var'))
```

```
  alpha = .2;
end
%--  display intermediate outputs
if(~exist('display','var'))
  display = true;
end

I = im2graydouble(I);

%-- Create a signed distance map (SDF) from mask
phi = mask2phi(init_mask);

%--main loop
for its = 1:max_ite   % Note: no automatic convergence test

  idx = find(phi <= 1.2 & phi >= -1.2);  %get the curve's narrow band

  %-- find interior and exterior mean
  upts = find(phi<=0);                 % interior points
  vpts = find(phi>0);                  % exterior points
  u = sum(I(upts))/(length(upts)+eps); % interior mean
  v = sum(I(vpts))/(length(vpts)+eps); % exterior mean

  F = (I(idx)-u).^2-(I(idx)-v).^2;         % force from image information
  curvature = get_curvature(phi,idx);  % force from curvature penalty

  dphidt = F./max(abs(F)) + alpha*curvature;  % gradient descent to minimize energy

  %-- maintain the CFL condition
  dt = .45/(max(dphidt)+eps);

  %-- evolve the curve
  phi(idx) = phi(idx) + dt.*dphidt;

  %-- Keep SDF smooth
  phi = sussman(phi, .5);

  %-- intermediate output
  if((display>0)&&(mod(its,20) == 0))
    showCurveAndPhi(I,phi,its);
  end
end

%-- final output
if(display)
  showCurveAndPhi(I,phi,its);
end

%-- make mask from SDF
```

```
  seg = phi<=0; %-- Get mask from levelset

  %--------------------------------------------------------------------
%--------------------------------------------------------------------


%-- Displays the image with curve superimposed
function showCurveAndPhi(I, phi, i)
  imshow(I,'initialmagnification',200,'displayrange',[0 255]); hold on;
  contour(phi, [0 0], 'g','LineWidth',4);
  contour(phi, [0 0], 'k','LineWidth',2);
  hold off;
  %title([num2str(i) ' Iterations']);
  drawnow;

%-- converts a mask to a SDF
function phi = mask2phi(init_a)
  phi=bwdist(init_a)-bwdist(1-init_a)+im2double(init_a)-.5;

%-- compute curvature along SDF
function curvature = get_curvature(phi,idx)
    [dimy, dimx] = size(phi);
    [y x] = ind2sub([dimy,dimx],idx);  % get subscripts

    %-- get subscripts of neighbors
    ym1 = y-1; xm1 = x-1; yp1 = y+1; xp1 = x+1;

    %-- bounds checking
    ym1(ym1<1) = 1; xm1(xm1<1) = 1;
    yp1(yp1>dimy)=dimy; xp1(xp1>dimx) = dimx;

    %-- get indexes for 8 neighbors
    idup = sub2ind(size(phi),yp1,x);
    iddn = sub2ind(size(phi),ym1,x);
    idlt = sub2ind(size(phi),y,xm1);
    idrt = sub2ind(size(phi),y,xp1);
    idul = sub2ind(size(phi),yp1,xm1);
    idur = sub2ind(size(phi),yp1,xp1);
    iddl = sub2ind(size(phi),ym1,xm1);
    iddr = sub2ind(size(phi),ym1,xp1);

    %-- get central derivatives of SDF at x,y
    phi_x  = -phi(idlt)+phi(idrt);
    phi_y  = -phi(iddn)+phi(idup);
    phi_xx = phi(idlt)-2*phi(idx)+phi(idrt);
    phi_yy = phi(iddn)-2*phi(idx)+phi(idup);
    phi_xy = -0.25*phi(iddl)-0.25*phi(idur)...
            +0.25*phi(iddr)+0.25*phi(idul);
    phi_x2 = phi_x.^2;
```

```
    phi_y2 = phi_y.^2;

    %-- compute curvature (Kappa)
    curvature = ((phi_x2.*phi_yy + phi_y2.*phi_xx - 2*phi_x.*phi_y.*phi_xy)./...
            (phi_x2 + phi_y2 +eps).^(3/2)).*(phi_x2 + phi_y2).^(1/2);

%-- Converts image to one channel (grayscale) double
function img = im2graydouble(img)
  [dimy, dimx, c] = size(img);
  if(isfloat(img)) % image is a double
    if(c==3)
      img = rgb2gray(uint8(img));
    end
  else          % image is a int
    if(c==3)
      img = rgb2gray(img);
    end
    img = double(img);
  end

%-- level set re-initialization by the sussman method
function D = sussman(D, dt)
  % forward/backward differences
  a = D - shiftR(D); % backward
  b = shiftL(D) - D; % forward
  c = D - shiftD(D); % backward
  d = shiftU(D) - D; % forward

  a_p = a;  a_n = a; % a+ and a-
  b_p = b;  b_n = b;
  c_p = c;  c_n = c;
  d_p = d;  d_n = d;

  a_p(a < 0) = 0;
  a_n(a > 0) = 0;
  b_p(b < 0) = 0;
  b_n(b > 0) = 0;
  c_p(c < 0) = 0;
  c_n(c > 0) = 0;
  d_p(d < 0) = 0;
  d_n(d > 0) = 0;

  dD = zeros(size(D));
  D_neg_ind = find(D < 0);
  D_pos_ind = find(D > 0);
  dD(D_pos_ind) = sqrt(max(a_p(D_pos_ind).^2, b_n(D_pos_ind).^2) ...
                  + max(c_p(D_pos_ind).^2, d_n(D_pos_ind).^2)) - 1;
  dD(D_neg_ind) = sqrt(max(a_n(D_neg_ind).^2, b_p(D_neg_ind).^2) ...
                  + max(c_n(D_neg_ind).^2, d_p(D_neg_ind).^2)) - 1;
```

```
  D = D - dt .* sussman_sign(D) .* dD;

%-- whole matrix derivatives
function shift = shiftD(M)
  shift = shiftR(M')';

function shift = shiftL(M)
  shift = [ M(:,2:size(M,2)) M(:,size(M,2)) ];

function shift = shiftR(M)
  shift = [ M(:,1) M(:,1:size(M,2)-1) ];

function shift = shiftU(M)
  shift = shiftL(M')';

function S = sussman_sign(D)
  S = D ./ sqrt(D.^2 + 1);
```

Published with MATLAB® R2018b

Appendix 7: Execution Time Evaluation MATLAB Code

```
% ========================================================================
% Read Coloured foot ulcer image and convert it to a grayscale Image
% Display the original Image
mycolourimage = imread('footulcer1.jpg');
myimage = rgb2gray(mycolourimage);

% Canny edge detection
tic
cannyedg = edge(myimage,'canny');
figure
imshow(cannyedg); title('cannyedg');
toc

%  Sobel Operator
% Display both horizontal and vertical Edges
tic
sobelvrthz = edge(myimage,'sobel','both');
figure
imshow(sobelvrthz); title('sobelvrthz');
toc

%  Roberts Operator
tic
robertsedg = edge(myimage,'roberts');
figure
imshow(robertsedg); title('robertsedg');
toc

%  Prewitt Operator
tic
prewittedg= edge(myimage,'prewitt');
figure
imshow(prewittedg); title('prewittedg');
toc

% Apply LOG edge detection
% The sigma used is 3
tic
f=fspecial('log',[15,15],3.0);
logedg1 = edge(myimage,'zerocross',[],f);
figure
imshow(logedg1); title('logedg1');
toc

% proposed Method
tic
ee=dfu_edgeFcnv2(myimage);
```

```
figure
imshow(ee)
toc
```

Appendix 8: PSNR Calculation MATLAB Code

```
function [ PSNR,mse]=psnr2(X,Y)



% If the second input Y is missing then the PSNR and MSE of X itself
%becomes the output (as if Y=0).

if nargin<2, D=X;
else
if any(size(X)~=size(Y)), error('The input size is not equal to each other!');
end
D=X-Y;
end
mse=sum(D(:).*D(:))/prod(size(X))
 PSNR=10*log10(255^2/mse)
```

Published with MATLAB® R2018b

Appendix 9: SSIM Calculation MATLAB Code

```
function [mssim, ssim_map] = ssim(img1, img2, K, window, L)

% ========================================================================
% SSIM Index with automatic downsampling, Version 1.0
% Copyright(c) 2009 Zhou Wang
% All Rights Reserved.
%
% ----------------------------------------------------------------------
% Permission to use, copy, or modify this software and its documentation
% for educational and research purposes only and without fee is hereby
% granted, provided that this copyright notice and the original authors'
% names appear on all copies and supporting documentation. This program
% shall not be used, rewritten, or adapted as the basis of a commercial
% software or hardware product without first obtaining permission of the
% authors. The authors make no representations about the suitability of
% this software for any purpose. It is provided "as is" without express
% or implied warranty.
%----------------------------------------------------------------------
%
%Input : (1) img1: the first image being compared
%       (2) img2: the second image being compared
%       (3) K: constants in the SSIM index formula (see the above
%           reference). defualt value: K = [0.01 0.03]
%       (4) window: local window for statistics (see the above
%           reference). default widnow is Gaussian given by
%           window = fspecial('gaussian', 11, 1.5);
%       (5) L: dynamic range of the images. default: L = 255
%
%Output: (1) mssim: the mean SSIM index value between 2 images.
%           If one of the images being compared is regarded as
%           perfect quality, then mssim can be considered as the
%           quality measure of the other image.
%
%Visualize the results:
%
%   mssim                   %Gives the mssim value
%   imshow(max(0, ssim_map).^4)  %Shows the SSIM index map
%========================================================================


if (nargin < 2 || nargin > 5)
   mssim = -Inf;
   ssim_map = -Inf;
   return;
end

if (size(img1) ~= size(img2))
```

```
  mssim = -Inf;
  ssim_map = -Inf;
  return;
end

[M N] = size(img1);

if (nargin == 2)
  if ((M < 11) || (N < 11))
                mssim = -Inf;
                ssim_map = -Inf;
    return
  end
  window = fspecial('gaussian', 11, 1.5);       %
  K(1) = 0.01;                                              % default settings
  K(2) = 0.03;                                              %
  L = 255;                                  %
end

if (nargin == 3)
  if ((M < 11) || (N < 11))
                mssim = -Inf;
                ssim_map = -Inf;
    return
  end
  window = fspecial('gaussian', 11, 1.5);
  L = 255;
  if (length(K) == 2)
    if (K(1) < 0 || K(2) < 0)
                              mssim = -Inf;
                          ssim_map = -Inf;
                          return;
    end
  else
                mssim = -Inf;
              ssim_map = -Inf;
                return;
  end
end

if (nargin == 4)
  [H W] = size(window);
  if ((H*W) < 4 || (H > M) || (W > N))
                mssim = -Inf;
                ssim_map = -Inf;
    return
  end
  L = 255;
  if (length(K) == 2)
```

```
    if (K(1) < 0 || K(2) < 0)
                                mssim = -Inf;
                            ssim_map = -Inf;
                            return;
    end
  else
                mssim = -Inf;
              ssim_map = -Inf;
                return;
  end
end

if (nargin == 5)
  [H W] = size(window);
  if ((H*W) < 4 || (H > M) || (W > N))
                mssim = -Inf;
                ssim_map = -Inf;
    return
  end
  if (length(K) == 2)
    if (K(1) < 0 || K(2) < 0)
                                mssim = -Inf;
                            ssim_map = -Inf;
                            return;
    end
  else
                mssim = -Inf;
              ssim_map = -Inf;
                return;
  end
end


img1 = double(img1);
img2 = double(img2);

% automatic downsampling
f = max(1,round(min(M,N)/256));
%downsampling by f
%use a simple low-pass filter
if(f>1)
   lpf = ones(f,f);
   lpf = lpf/sum(lpf(:));
   img1 = imfilter(img1,lpf,'symmetric','same');
   img2 = imfilter(img2,lpf,'symmetric','same');

   img1 = img1(1:f:end,1:f:end);
   img2 = img2(1:f:end,1:f:end);
end
```

```
C1 = (K(1)*L)^2;
C2 = (K(2)*L)^2;
window = window/sum(sum(window));

mu1   = filter2(window, img1, 'valid');
mu2   = filter2(window, img2, 'valid');
mu1_sq = mu1.*mu1;
mu2_sq = mu2.*mu2;
mu1_mu2 = mu1.*mu2;
sigma1_sq = filter2(window, img1.*img1, 'valid') - mu1_sq;
sigma2_sq = filter2(window, img2.*img2, 'valid') - mu2_sq;
sigma12 = filter2(window, img1.*img2, 'valid') - mu1_mu2;

if (C1 > 0 && C2 > 0)
   ssim_map = ((2*mu1_mu2 + C1).*(2*sigma12 + C2))./((mu1_sq + mu2_sq + C1).*(sigma1_sq + sigma2_sq + C2));
else
   numerator1 = 2*mu1_mu2 + C1;
   numerator2 = 2*sigma12 + C2;
                denominator1 = mu1_sq + mu2_sq + C1;
   denominator2 = sigma1_sq + sigma2_sq + C2;
   ssim_map = ones(size(mu1));
   index = (denominator1.*denominator2 > 0);
   ssim_map(index) = (numerator1(index).*numerator2(index))./(denominator1(index).*denominator2(index));
   index = (denominator1 ~= 0) & (denominator2 == 0);
   ssim_map(index) = numerator1(index)./denominator1(index);
end

mssim = mean2(ssim_map);

return
```

Published with MATLAB® R2018b